

1 Multi-model ensemble simulations of olive pollen 2 distribution in Europe in 2014: current status and outlook.

3 Mikhail Sofiev¹, Olga Ritenberga², Roberto Albertini³, Joaquim Arteta⁴, Jordina Belmonte^{5,6}, Carmi
4 Geller Bernstein⁷, Maira Bonini⁸, Sevcan Celenk⁹, Athanasios Damialis^{10,11}, John Douros¹²,
5 Hendrik Elbern¹³, Elmar Friese¹³, Carmen Galan¹⁴, Gilles Oliver¹⁵, Ivana Hrga¹⁶, Rostislav
6 Kouznetsov¹, Kai Krajsek¹⁷, Donat Magyar¹⁸, Jonathan Parmentier⁴, Matthieu Plu⁴, Marje Prank¹,
7 Lennart Robertson¹⁹, Birthe Marie Steensen²⁰, Michel Thibaudon¹⁵, Arjo Segers²¹, Barbara
8 Stepanovich¹⁶, Alvaro M. Valdebenito²⁰, Julius Vira¹, Despoina Vokou¹¹

9
10 ¹ Finnish Meteorological Institute, Erik Palménin Aukio 1, Finland

11 ² University of Latvia, Latvia

12 ³ Department of Medicine and Surgery, University of Parma, Italy

13 ⁴ CNRM UMR 3589, Météo-France/CNRS, Toulouse, France

14 ⁵ Institute of Environmental Sciences and Technology (ICTA), Universitat Autònoma de Barcelona,
15 Spain

16 ⁶ Department of Animal Biology, Plant Biology and Ecology, Universitat Autònoma de Barcelona,
17 Spain

18 ⁷ Sheba Medical Center, Ramat Gan Zabludowicz Center for Autoimmune Diseases, Israel

19 ⁸ Agenzia Tutela della Salute della Città Metropolitana di Milano/ LHA ATS Città Metropolitana
20 Milano, Italy

21 ⁹ Biology department, Uludag University, Turkey

22 ¹⁰ Chair and Institute of Environmental Medicine, UNIKA-T, Technical University of Munich and
23 Helmholtz Zentrum München - German Research Center for Environmental Health, Augsburg,
24 Germany

25 ¹¹ Department of Ecology, School of Biology, Aristotle University of Thessaloniki, Greece

26 ¹² Royal Netherlands Meteorological Institute, De Bilt, The Netherlands

27 ¹³ Rhenish Institute for Environmental Research at the University of Cologne, Germany

28 ¹⁴ University of Cordoba, Spain

29 ¹⁵ RNSA, Brussieu, France

30 ¹⁶ Andrija Stampar Teaching Institute of Public Health, Croatia

31 ¹⁷ Institute of Energy and Climate Research (IEK-8), Forschungszentrum Jülich, Germany

32 ¹⁸ National Centre of Public Health, Hungary

33 ¹⁹ Swedish Meteorological and Hydrological Institute SMHI, Sweden

34 ²⁰ MET Norway

35 ²¹ TNO, Netherlands

36

37 1. Abstract

38 The paper presents the first modelling experiment of the European-scale olive pollen dispersion,
39 analyses the quality of the predictions and outlines the research needs. A 6-models strong ensemble

40 of Copernicus Atmospheric Monitoring Service (CAMS) was run through the season of 2014
41 computing the olive pollen distribution. The simulations have been compared with observations in 8
42 countries, members of the European Aeroallergen Network (EAN). Analysis was performed for
43 individual models, the ensemble mean and median, and for a dynamically optimized combination of
44 the ensemble members obtained via fusion of the model predictions with observations. The models,
45 generally reproducing the olive season of 2014, showed noticeable deviations from both
46 observations and each other. In particular, the season start was reported too early, by 8 days, but for
47 some models the error mounted to almost two weeks. For the season end, the disagreement between
48 the models and the observations varied from a nearly perfect match up to two weeks too late. A
49 series of sensitivity studies performed to understand the origin of the disagreements revealed crucial
50 role of ambient temperature and consistency of its representation by the meteorological models and
51 by the heat-sum-based phenological model. In particular, a simple correction to the heat sum
52 threshold eliminated the season-start shift but its validity in other years remains to be checked. The
53 short-term features of the concentration time series were reproduced better suggesting that the
54 precipitation events and cold/warm spells, as well as the large-scale transport were represented
55 rather well. Ensemble averaging led to more robust results. The best skill scores were obtained with
56 data fusion, which used the previous-days observations to identify the optimal weighting
57 coefficients of the individual model forecasts. Such combinations were tested for the forecasting
58 period up to 4 days and shown to remain nearly optimal throughout the whole period.

59

60 **Keywords:** olive pollen, airborne pollen modelling, pollen forecasting, multi-model ensemble, data
61 fusion, aerobiology

62

63 2. Introduction

64 Biogenic aerosols, such as pollen and spores, constitute a substantial fraction of particulate matter
65 mass in the air during the vegetation flowering season and can have strong health effects causing
66 allergenic rhinitis and asthma (G D'Amato et al., 2007). One of important allergenic trees is olive.

67 Olive is one of the most extensive crops and its oil is one of the major economic resources in
68 Southern Europe. The bulk of olive habitation (95% of the total area worldwide) is concentrated in
69 the Mediterranean basin (Barranco et al., 2008). Andalusia has by far the world's largest area given
70 over to olive plantations, 62% of the total olive land of Spain and 15% of the world's plantations
71 (Gómez et al., 2014).

72 Olive pollen is also one of the most important causes of respiratory allergies in the Mediterranean
73 basin (G. D'Amato et al., 2007) and in Andalusia it is considered as the main cause of allergy. In

74 Cordoba City (S Spain), 71-73% of pollen-allergy sufferers are sensitive to olive pollen (Sánchez-
75 Mesa et al., 2005), (Cebrino et al., 2017). High rates of sensitization to olive pollen have been
76 documented in Mediterranean countries: 44% in Spain and 20% in Portugal (Pereira et al., 2006),
77 31.8% in Greece (Gioulekas et al., 2004), 27.5% in Portugal (Loureiro et al., 2005), 24% in Italy
78 (Negrini et al., 1992), 21.6% in Turkey (Kalyoncu et al., 1995), and 15% in France (Spieksma,
79 1990). At the same time, relations between allergy and pollen concentrations is person- and case-
80 specific: allergen content of the pollen grains varies from year to year and day to day, as well as the
81 individual sensitivity of allergy sufferers (de Weger et al., 2013; Galan et al., 2013)

82 Olive is an entomophilous species that presents a secondary anemophily, favored by the agricultural
83 management during the last centuries. This tree is very well adapted to the Mediterranean climate
84 and tolerates the high summer and the low winter temperatures, as well as the summer drought,
85 characteristic for this climate.

86 Olive floral phenology is characterized by bud formation during summer, dormancy during autumn,
87 budburst in late winter, and flowering in late spring (Fernandez-Escobar et al., 1992; Galán et al.,
88 2005; García-mozo et al., 2006). Similar to some other trees, olive flowering intensity shows
89 alternated years with high and low or even no pollen production. The characteristic quasi-biannual
90 cycles are well visible in observations (Ben Dhiab et al., 2016; Garcia-Mozo et al., 2014). This
91 cycle, similar to other trees, e.g., birch, is not strict and is frequently interrupted showing several
92 years with similar flowering intensity (Garcia-Mozo et al., 2014). Such cyclic behavior is related to
93 the reproductive development, which is completed in two consecutive years. In the first year, the
94 bud vegetative or reproductive character is determined by the current harvest level, since this is the
95 main factor responsible for the inter-annual variation of flowering. In the second year, after the
96 winter rest, the potentially reproductive buds that have fulfilled their chilling requirements develop
97 into inflorescences (Barranco et al., 2008).

98 After the bud break, certain bio-thermic units are required for the development of the
99 inflorescences. Both the onset of the heat accumulation period and the temperature threshold for the
100 amount of positive heat units might vary according to the climate of a determined geographical
101 area. The threshold level was also reported to decrease towards the north (Aguilera et al., 2013).
102 Altitude is the topographical factor most influencing olive local phenology and the major weather
103 factors are temperature, rainfall, and solar radiation that control the plant evapotranspiration (Oteros
104 et al., 2013; Oteros et al., 2014).

105 Several studies used airborne pollen as a predictor variable for determining the potential sources of
106 olive pollen emission, e.g. Concentric Ring Method (J. Oteros et al., 2015; Rojo et al., 2016),

107 geostatistical techniques (Rojo and Pérez-Badia, 2015) and the spatio-temporal airborne pollen
108 maps (Aguilera et al., 2015).

109 There is a substantial variability of olive biological characteristics and its responses to
110 environmental stresses. In particular, the allergen content was shown to be strongly different in
111 pollen coming from different parts of the Iberian Peninsula (Galan et al., 2013).

112 Forecasting efforts of the olive pollen season were mainly concentrated on statistical models
113 predicting the season start and peak using various meteorological predictors. The bulk of studies is
114 based on information from one or a few stations within a limited region (e.g., Orlandi et al., (2006),
115 Moriondo et al., (2001), Alba and Diaz De La Guardia, (1998), Frenguelli et al., (1989), Galán et
116 al., (2005), Fornaciari et al., (1998), etc.). Several wider-area studies were also performed aiming at
117 more general statistical characteristics of the season, e.g. (Aguilera et al., 2014, 2013; Galan et al.,
118 2016).

119 Numerical modelling of olive pollen transport is very limited. In fact, the only regional-scale
120 computations regularly performed since 2008 were made by the SILAM model (<http://silam.fmi.fi>)
121 but the methodology was only scarcely outlined in (Galan et al., 2013).

122 Copernicus Atmospheric Monitoring Service CAMS (<http://atmosphere.copernicus.eu>) is one of the
123 services of the EU Copernicus program, addressing various global and regional aspects of
124 atmospheric state and composition. CAMS European air quality ensemble (Marécal et al., 2015)
125 provides high-resolution forecasts and reanalysis of the atmospheric composition over Europe.
126 Olive pollen is one of the components, which are being introduced in the CAMS European
127 ensemble in co-operation with European Aeroallergen Network EAN
128 (<https://www.polleninfo.org/country-choose.html>).

129 One of possible ways of improving the quality of model predictions without direct application of
130 data assimilation is to combine them with observations via ensemble-based data fusion methods
131 (Potemski and Galmarini, 2009). Their efficiency has been demonstrated for air quality problems
132 (Johansson et al., 2015 and references therein) and climatological models (Genikhovich et al., 2010)
133 but the technology has never been applied to pollen.

134 The aim of the current publication is to present the first Europe-wide ensemble-based evaluation of
135 the olive pollen dispersion during the season of 2014. The study followed the approach of the multi-
136 model simulations for birch (Sofiev et al., 2015) with several amendments reflecting the peculiarity
137 of olive pollen distribution in Europe. We also made further steps towards fusion of model
138 predictions and observations and demonstrate its value in the forecasting regime.

139 The next section will present the participating models and setup of the simulations, the observation
140 data used for evaluation of the model predictions, approach for constructing an optimised multi-
141 model ensemble, and a list of sensitivity computations. The Results section will present the
142 outcome of the simulations and the quality scores of the individual models and the ensemble. The
143 Discussion section will be dedicated to analysis of the results, considerations of the efficiency of the
144 multi-model ensemble for olive pollen, and identification of the development needs.

145 3. Materials and methods

146 This section presents the regional models used in the study, outlines the olive pollen source term
147 implemented in all of them, and pollen observations used for evaluation of the model predictions.

148 3.1. Dispersion models

149 The dispersion models used in the study comprise the CAMS European ensemble, which is
150 described in details by Marécal et al., (2015) and (Sofiev et al., 2015). Below, only the model
151 features relevant for the olive pollen atmospheric transport calculations are described.

152 The ensemble consisted of six models.

153 **EMEP** model of EMEP/MSC-West (European Monitoring and Evaluation Programme /
154 Meteorological Synthesizing Centre - West) is a chemical transport model developed at the
155 Norwegian Meteorological Institute and described in Simpson et al., (2012). It is flexible with
156 respect to the choice of projection and grid resolution. Dry deposition is handled in the lowest
157 model layer. A resistance analogy formulation is used to describe dry deposition of gases, whereas
158 for aerosols the mass-conservative equation is adopted from Venkatram, (1978) with the dry
159 deposition velocities dependent on the land use type. Wet scavenging is dependent on precipitation
160 intensity and is treated differently within and below cloud. The below-cloud scavenging rates for
161 particles are based on Scott, (1979). The rates are size-dependent, growing for larger particles.

162 **EURAD-IM** (<http://www.eurad.uni-koeln.de>) is an Eulerian meso-scale chemistry transport model
163 involving advection, diffusion, chemical transformation, wet and dry deposition and sedimentation
164 of tropospheric trace gases and aerosols (Hass et al., 1995; Memmesheimer et al., 2004). It includes
165 3D-VAR and 4D-VAR chemical data assimilation (Elbern et al., 2007) and is able to run in nesting
166 mode. The positive definite advection scheme of Bott (1989) is used to solve the advective transport
167 and the aerosol sedimentation. An eddy diffusion approach is applied to parameterize the vertical

168 sub-grid-scale turbulent transport (Holtslag and Nieuwstadt, 1986). Dry deposition of aerosol
169 species is treated size-dependent using the resistance model of Petroff and Zhang (2010). Wet
170 deposition of pollen is parameterized according to Baklanov and Sorensen (2001).

171 **LOTOS-EUROS** (<http://www.lotos-euros.nl/>) is an Eulerian chemical transport model (Schaap et
172 al., 2008). The advection scheme follows Walcek and Aleksic (1998). The dry deposition scheme of
173 Zhang et al. (2001) is used to describe the surface uptake of aerosols. Below-cloud scavenging is
174 described using simple scavenging coefficients for particles (Simpson et al., 2003).

175 **MATCH** (<http://www.smhi.se/en/research/research-departments/air-quality/match-transport-and-chemistry-model-1.6831>)
176 is an Eulerian multi-scale chemical transport model with mass-
177 conservative transport and diffusion based on a Bott-type advection scheme (Langner et al., 1998;
178 Robertson and Langner, 1999). For olive pollen, dry deposition is mainly treated by sedimentation
179 and a simplified wet scavenging scheme is applied. The temperature sum, which drives pollen
180 emission, is computed off-line starting from January onwards and is fed into the emission module.

181 **MOCAGE** (http://www.cnrm.meteo.fr/gmgec-old/site_engl/mocage/mocage_en.html) is a multi-
182 scale dispersion model with grid-nesting capability (Josse et al., 2004; Martet et al., 2009). The
183 semi-Lagrangian advection scheme of Williamson and Rasch (1989) is used for the grid-scale
184 transport. The convective transport is based on the parameterization proposed by Bechtold et al.
185 (2001) whereas the turbulent diffusion follows the parameterization of Louis (1979). Dry deposition
186 including the sedimentation scheme follows Seinfeld and Pandis (1998). The wet deposition by the
187 convective and stratiform precipitations is based on Giorgi and Chameides (1986).

188 **SILAM** (<http://silam.fmi.fi>) is a meso-to-global scale dispersion model (Sofiev et al., 2015), also
189 described in the review of Kukkonen et al. (2012). Its dry deposition scheme (Kouznetsov and
190 Sofiev, 2012) is applicable for a wide range of particle sizes including coarse aerosols, which are
191 primarily removed by sedimentation. The wet deposition parameterization distinguishes between
192 sub- and in-cloud scavenging by both rain and snow (Sofiev et al., 2006). For coarse particles,
193 impaction scavenging parameterised following (Kouznetsov and Sofiev, 2012) is dominant below
194 the cloud. The model includes emission modules for six pollen types: birch, olive, grass, ragweed,
195 mugwort, and alder, albeit only birch, ragweed, and grass sources are so-far described in the
196 literature (Prank et al., 2013; Sofiev, 2016; Sofiev et al., 2012).

197 Three **ENSEMBLE** models were generated by (i) arithmetic average, (ii) median and (iii) optimal
198 combination of the 6 model fields. Averaging and median were taken on hourly basis, whereas
199 optimization was applied at daily level following the temporal resolution of the observational data.

200 For the current work, we used simple linear combination c_{opt} of the models c_m , $m=1..M$ minimising
 201 the regularised RMSE J of the optimal field:

$$202 \quad (1) \quad c_{opt}(i, j, k, t, \tau, A) = a_0(\tau) + \sum_{m=1}^M a_m(\tau) c_m(i, j, k, t), \quad A = [a_1..a_M], \quad a_m \geq 0 \quad \forall m$$

$$203 \quad (2) \quad J(t, \tau) = \text{sqr}t \left[\frac{1}{O} \sum_{o=1}^O (c_{opt}(i_o, j_o, k_o, t, \tau, A) - c_o(t))^2 \right] +$$

$$\alpha \sum_{m=1}^M \left(a_m(\tau) - \frac{1}{M} \right)^2 + \beta \sum_{m=1}^M (a_m(\tau-1) - a_m(\tau))^2, \quad \tau = \{d_{-k}, d_0\}$$

204 Here, i, j, k, t are indices along the x,y,z, and time axes, M is the number of models in the ensemble, O
 205 is the number of observation stations, $\tau = \{d_{-k}:d_0\}$ is the time period of $k+1$ days covered by the
 206 analysis window, starting from d_{-k} until d_0 , $\tau - 1$ is the previous-day analysis period $\tau - 1 = \{d_{-k-1}:d_{-1}\}$,
 207 c_m is concentration of pollen predicted by the model m , c_o is observed pollen concentration, a_m is
 208 time-dependent weight coefficient of the model m in the ensemble, a_0 is time-dependent bias
 209 correction. In the Eq. (2), the first term represents the RMSE of the assimilated period τ , the second
 210 term limits the departure of the coefficients from the homogeneous weight distribution, the third
 211 one limits the speed of evolution of the a_m coefficients in time. The scaling values α and β decide
 212 on the strength of regularization imposed by these two terms.

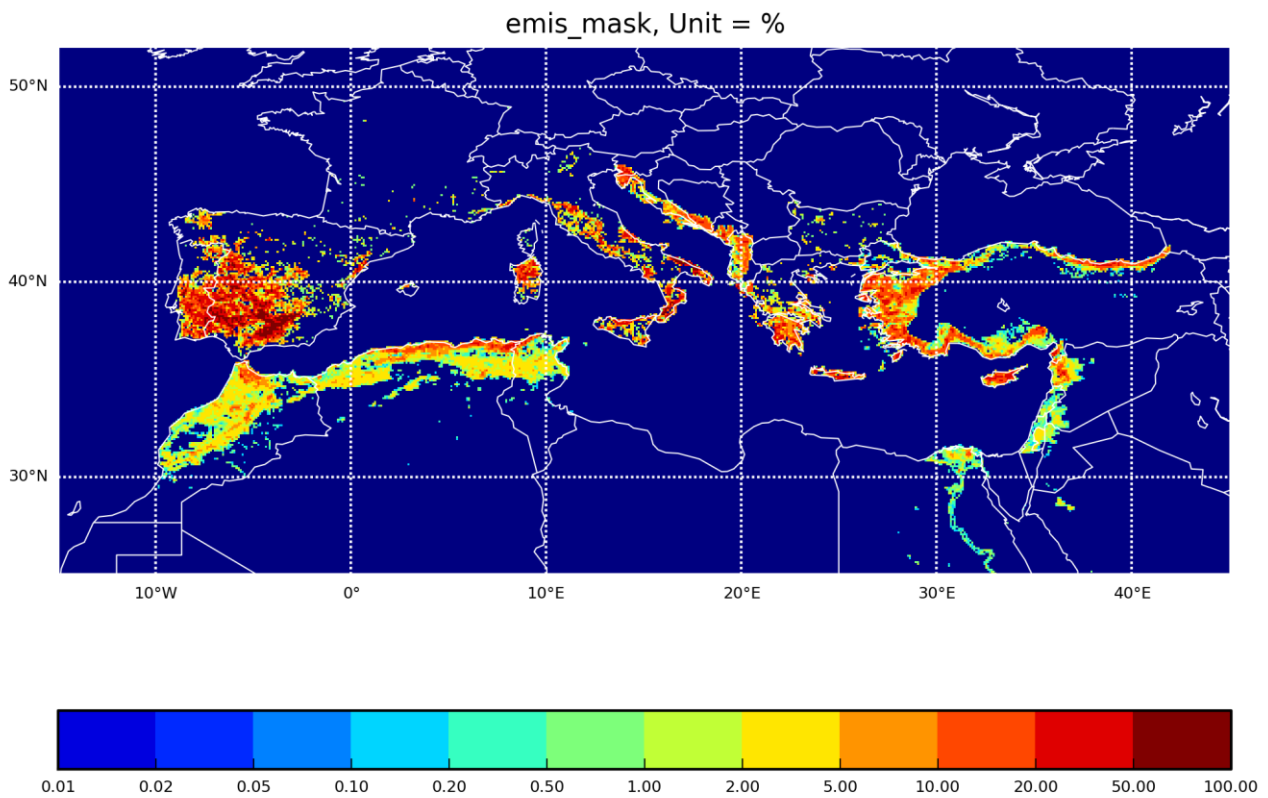
213 The ensemble was constructed mimicking the forecasting mode. Firstly, the analysis is made using
 214 data from the analysis period τ . The obtained weighting coefficients a_i are used over several days
 215 forwards from day d_0 : from d_1 until d_{nf} , which constitute the forecasting steps. The performance of
 216 the ensemble is evaluated for each length of the forecast, from 1 to n_f days.

217 3.2.Olive pollen source term

218 All models of this study are equipped with the same olive pollen source term, which has not been
 219 described in the scientific literature yet. However, it follows the same concept as the birch source
 220 (Sofiev et al., 2012) that was used for the birch ensemble simulations (Sofiev et al., 2015). The
 221 formulations and input data are open at <http://silam.fmi.fi/MACC>. The main input dataset is the
 222 annual olive pollen production map based on ECOCLIMAP dataset (Champeaux et al., 2005;
 223 Masson et al., 2003), Figure 1.

224 ECOCLIMAP incorporates the CORINE land-cover data for most of western-European countries
 225 with explicit olive-plantations land-use type (CEC, 1993). For Africa and countries missing from

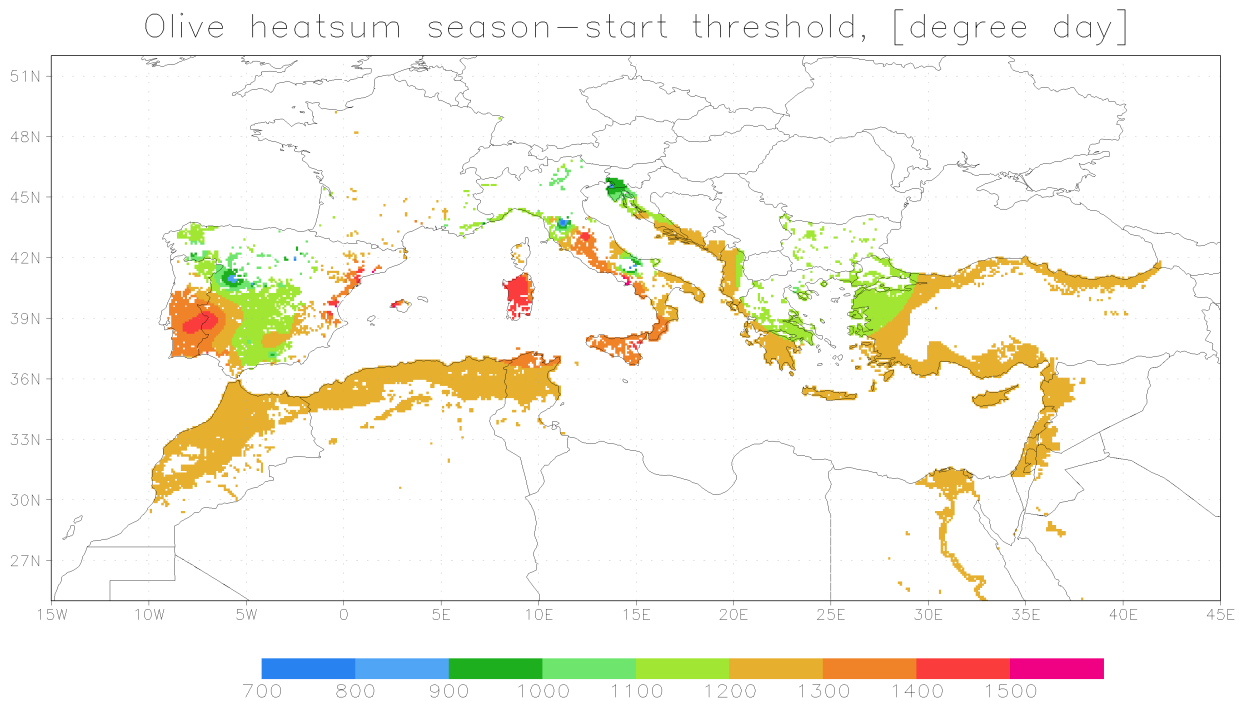
226 CORINE, the empty areas were filled manually assuming that 10% of all tree-like land-use types
 227 are olives. This way, Tunisian, Egyptian, and Algerian olive plantations were recovered and
 228 included in the inventory. In some areas, such as France (Figure 1), the olive habitat looks
 229 unrealistically low, probably because the large olive plantations are rare but the trees are planted in
 230 private gardens, city park areas, streets, etc. Since these distributed sources are not reflected in the
 231 existing land-use inventories, they are not included in the current pollen production map.
 232



233
 234 **Figure 1.** Olive pollen habitat map, percentage of the area occupied by the trees, [%]. Productivity of an area with
 235 100% olive coverage is assumed to be 10^{10} pollen grain m^{-2} season $^{-1}$.

236
 237 Similar to birch, the flowering description follows the concept of Thermal Time phenological
 238 models and, in particular, the double-threshold air temperature sum approach of Linkosalo et al.
 239 (2010) modified by Sofiev et al. (2012). Within that approach, the heat accumulation starts on a
 240 prescribed day in spring (1 January in the current setup – after Spano et al. (1999), Moriondo et al.
 241 (2001), Orlandi et al. (2005a, 2005b)) and continues throughout spring. The cut-off daily
 242 temperature below which no summation occurs is 0°C, as compares to 3.5°C for birch. It was
 243 obtained from the multi-annual fitting of the season start. Flowering starts when the accumulated
 244 heat reaches the starting threshold (Figure 2) and continues until the heat reaches the ending

245 threshold (in the current setup, equal to the start-season threshold + 275 degree day). The rate of
246 heat accumulation is the main controlling parameter for pollen emission: the model assumes direct
247 proportionality between the flowering stage and fraction of the heat sum accumulated to-date.



248 GrADS: COLA/IGES 2016-12-13-10:57

249 **Figure 2.** Heat sum threshold for the start of the season. Unit = [degree day]

250

251 Similar to birch parameterization of Sofiev et al. (2012), the model distinguishes between the pollen
252 maturation, which is solely controlled by the heat accumulation described above, and pollen release,
253 which depends on other parameters. Higher relative humidity (RH) and rain reduce the release,
254 completely stopping it for $RH > 80\%$ and/or $rain > 0.1 \text{ mm hr}^{-1}$. Strong wind promotes it by up to
255 50%. Atmospheric turbulence is taken into account via the turbulent velocity scale and thus
256 becomes important only in cases close to free convection. In stable or neutral stratification and calm
257 conditions the release is suppressed by 50%. The interplay between the pollen maturation and
258 release is controlled by an intermediate ready-pollen buffer, which is filled-in by the maturation and
259 emptied by the release flows.

260 Local-scale variability of flowering requires probabilistic description of its propagation (Siljamo et
261 al., 2008). In the simplest form, the probability of an individual tree entering the flowering stage can
262 be considered via the uncertainty of the temperature sum threshold determining the start of

263 flowering for the grid cell – 10% in the current simulations. The end of the season is described via
264 the open-pocket principle: the flowering continues until the initially available amount of pollen is
265 completely released. The uncertainty of this number is taken to be 10% as well.

266

267 3.3. Pollen observations

268 The observations for the model evaluation in 2014 have been provided by the following 6 national
269 networks, members of the European Aeroallergen Network (EAN): Croatia, Greece, France,
270 Hungary, Israel, Italy, Spain, and Turkey. The data were screened for completeness and existence of
271 non-negligible olive season: (i) time series should have at least 30 valid observations, (ii) at least 10
272 daily values during the season should exceed 3 pollen m^{-3} , and (iii) the seasonal pollen index (SPI,
273 an integral of the concentrations over the whole season) should be at least 25 pollen day m^{-3} . After
274 this screening, information of 62 sites was used in the intercomparison. Data from Hungary referred
275 to 2016 and required dedicated computations for evaluating the long-range transport events.

276 Pollen monitoring was performed with Burkard 7-day and Lanzoni 2000 pollen traps based on the
277 Hirst design (Hirst, 1952). The pollen grains were collected at an airflow rate of 10 l min^{-1} . The
278 observations covered the period from March until September, with some variations between the
279 countries. Daily pollen concentrations were used. Following the EAS-EAN requirements (Galán et
280 al., 2014; Jäger et al., 1995), most samplers were located at heights of between 10m and 30m on the
281 roofs of suitable buildings. The places were frequently downtown of the cities, i.e. largely represent
282 the urban-background conditions (not always though). With regard to microscopic analysis, the
283 EAS-EAN requirement is to count at least 10% of the sample using horizontal or vertical strips
284 (Galán et al., 2014). The actual procedures vary between the countries but generally comply. The
285 counting in 2014 was mainly performed along four horizontal traverses as suggested by Mandrioli
286 et al., (1998). In all cases, the data were expressed as mean daily concentrations (pollen m^{-3}).

287 3.4. Setup of the simulations

288 Simulations followed the standards of CAMS European ensemble (Marécal et al., 2015). The
289 domain spanned from 25°W to 45°E and from 30°N to 70°N. Each of the 6 models was run with its
290 own horizontal and vertical resolutions, which varied from 0.1° to 0.25° of the horizontal grid cell
291 size, and had from 3 up to 52 vertical layers within the troposphere (Table 1). This range of
292 resolutions is not designed to reproduce local aspects of pollen distribution, instead covering the

293 whole continent and describing the large-scale transport. The 10km grid cells reach the sub-city
 294 scale but still insufficient to resolve the valleys and individual mountain ridges. The limited number
 295 of vertical dispersion layers used by some models is a compromise allowing for high horizontal
 296 resolution. Thick layers are not a major limitation as long as the full vertical resolution of the input
 297 meteorological data is used for evaluation of dispersion parameters (Sofiev, 2002).

298 The simulations were made retrospectively for the season of 2014 starting from 1 January (the
 299 beginning of the heat sum accumulation) until 30 June when the pollen season was over. All models
 300 produced hourly output maps with concentrations at 8 vertical levels (near surface, 50, 250, 500,
 301 1000, 2000, 3000 and 5000 metres above the surface), as well as dry and wet deposition maps.

302 All models considered pollen as an inert water-insoluble particle 28 μm in diameter and with a
 303 density of 800 kg m^{-3} .

304

305

306 **Table 1.** Setup of the simulations for the participating models

Model	Horizontal dispersion grid	Dispersion vertical	Meteo input	Meteo grid	Meteo vertical
EMEP	0.25° × 0.125°	20 levels up to 100 hPa	ECMWF IFS 00 operational forecast, internal preprocessor	0.25° × 0.125°	IFS lvs 39 – 91 up to 100 hPa
EURAD-IM	15 km, Lambert conformal proj.	23 layers up to 100 hPa	WRF based on ECMWF IFS	Same as CTM	Same as CTM
LOTOS-EUROS	0.25° × 0.125°	3 dyn. lvs up to 3.5km, sfc 25m	ECMWF IFS 00 operational forecast, internal preprocessor	0.5° × 0.25°	IFS lvs 69-91 up to 3.5km
MATCH	0.2° × 0.2°	52 layers up to 7 km	ECMWF IFS 00 from MARS, internal preprocessor	0.2° × 0.2°	IFS vertical: 91 lvs
MOCAGE	0.2° × 0.2°	47 layers up to 5hPa (7 in ABL)	ECMWF IFS 00 operational forecast, internal preprocessor	0.125° × 0.125°	IFS vertical 91 lvs
SILAM	0.1° × 0.1°	9 layers up to 7.5 km	ECMWF IFS 00 operational forecast, internal preprocessor	0.125° × 0.125°	IFS lvs 62-137 up to ~110hPa

307

308

309 4. Results for the pollen season of 2014

310 4.1. Observed peculiarities of the season

311 At French Mediterranean stations (Aix-en-Provence, Avignon, Montpellier, Nice, Nîmes and
312 Toulon), the mean value of the Seasonal Pollen Index (SPI) in 2014 was quite similar to that of
313 2012 but lower than in 2013 (see (de Weger et al., 2013) for the SPI relevance to allergy).

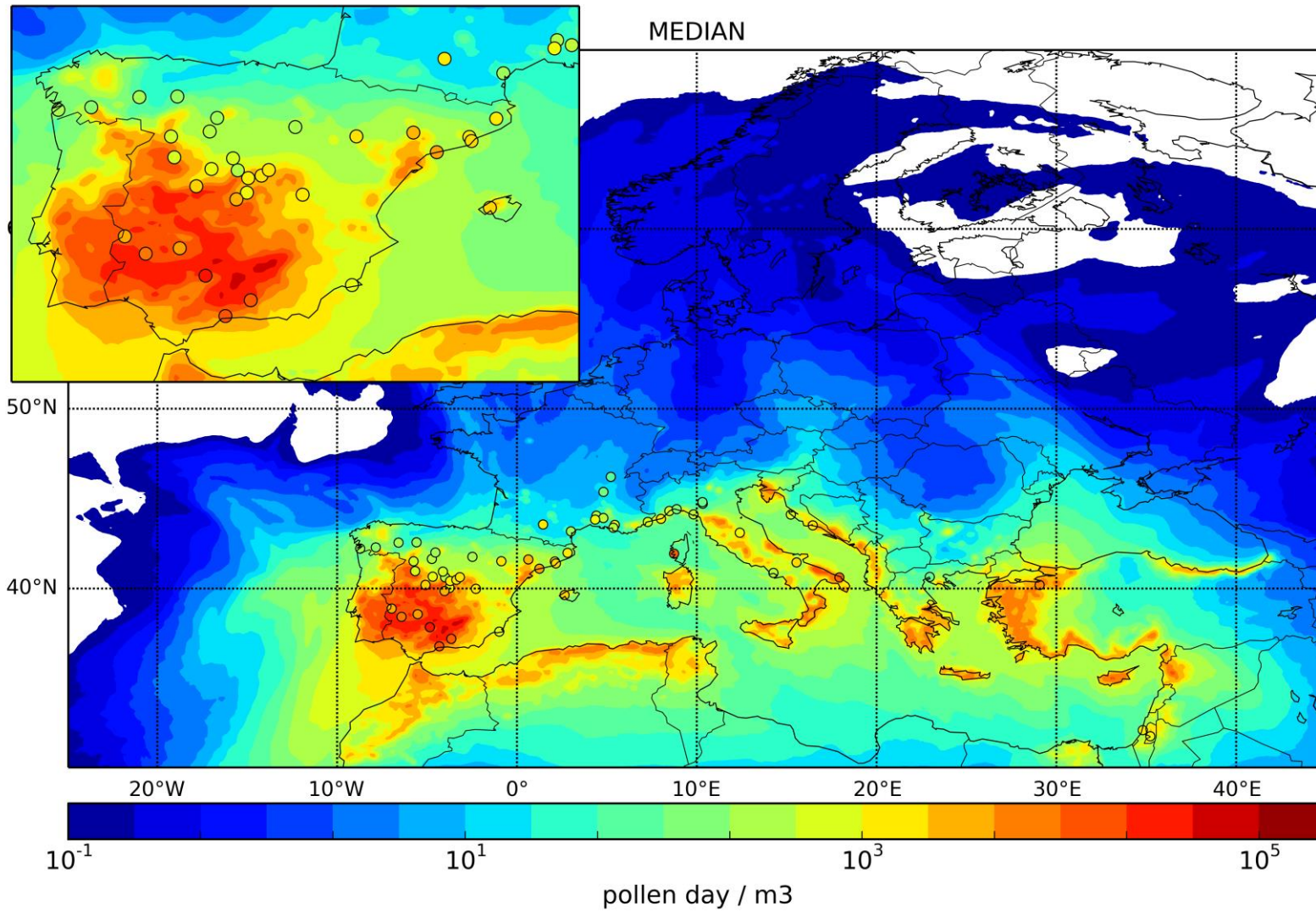
314 The start of the pollen season was earlier than in the previous five years. The duration of the season
315 has been the longest one on Aix-en-Provence, Nice and Nîmes since 2010. On Ajaccio (Corsica)
316 station, the SPI was higher in 2014 than at other stations, similar to the situation in 2012.

317 In Andalusia, 2014 was the second warmest year during the last decades but more humid than usual,
318 5% above the typical relative humidity level (<https://www.ncdc.noaa.gov/sotc/global/201413>).
319 However, after an intense olive flowering in 2013, in 2014 the flowering intensity was lower and
320 similar to 2012, in agreement with the bi-annual alterations of the season severity.

321 In Northern Italy, the 2014 olive pollen season was less intense than the average of the previous ten
322 years (2004-2013). Instead, in Southern Italy, the 2014 season was more intense in the first part and
323 less intense in the second part (after the beginning of June) than during previous seasons. No
324 differences were noted with respect to the start and the end of the season in both cases.

325 In Thessaloniki, Greece, in 2014, the pollen season started in the same time as during the last
326 decades (first half of April), but ended about 1.5 month later (last half of October). The pollen
327 season peak has been steadily in May. The SPI was considerably higher in 2014 (418 pollen day m⁻³
328 ³), compared against the previous two years (approximately 300 pollen day m⁻³). The overall shape
329 of the pollen season in 2014 resembled the ones during the last decade, however, with a multi-
330 modal and less peaky pattern.

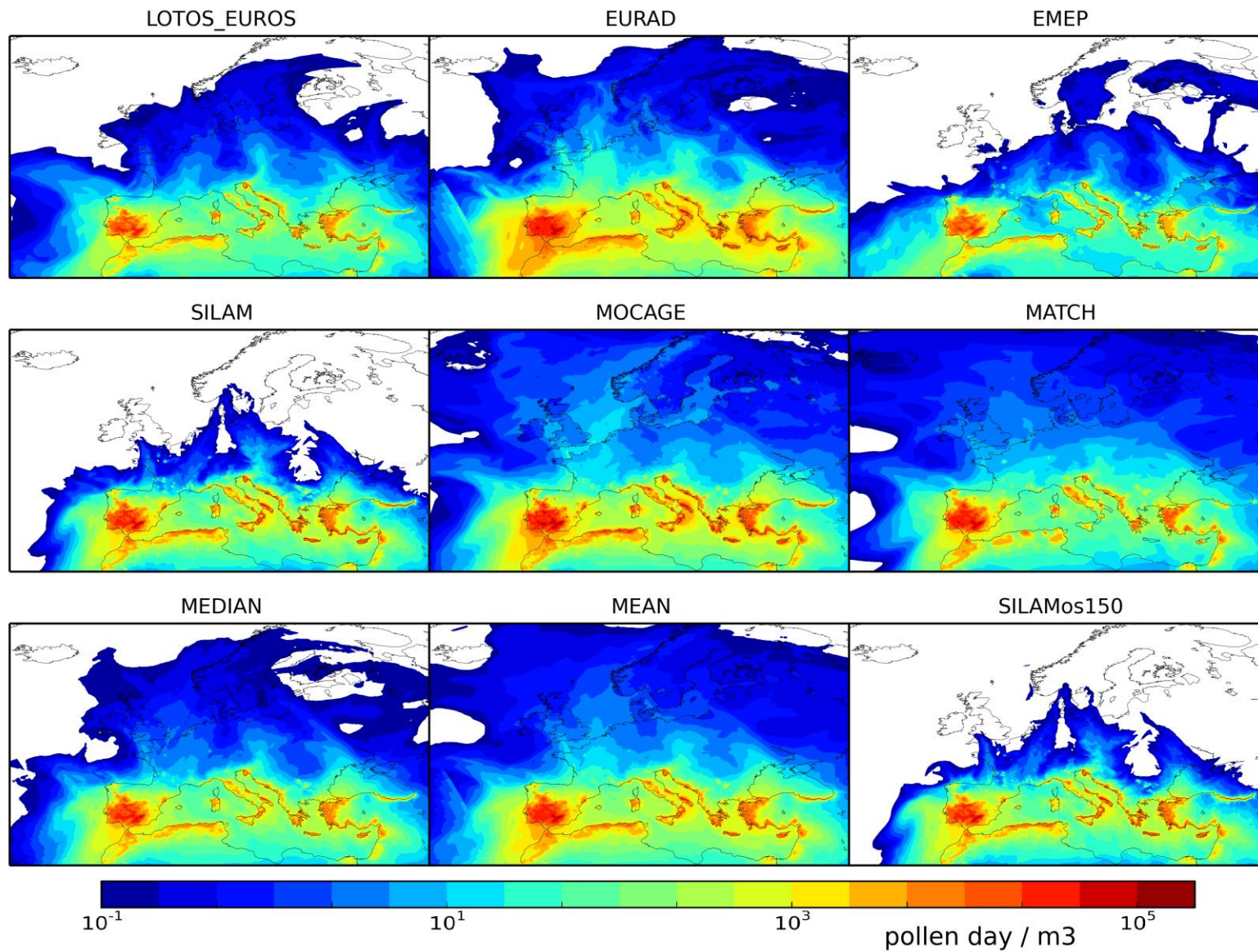
331



332

333 **Figure 3.** Observed (dots) and MEDIAN-model predicted (shades) Seasonal Pollen Index (SPI, sum of daily concentrations), 2014, [pollen day m⁻³].

334



335
 336 **Figure 4.** Modelled Seasonal Pollen Index (SPI) by the individual ensemble members and mean models, 2014, [pollen day m⁻³].

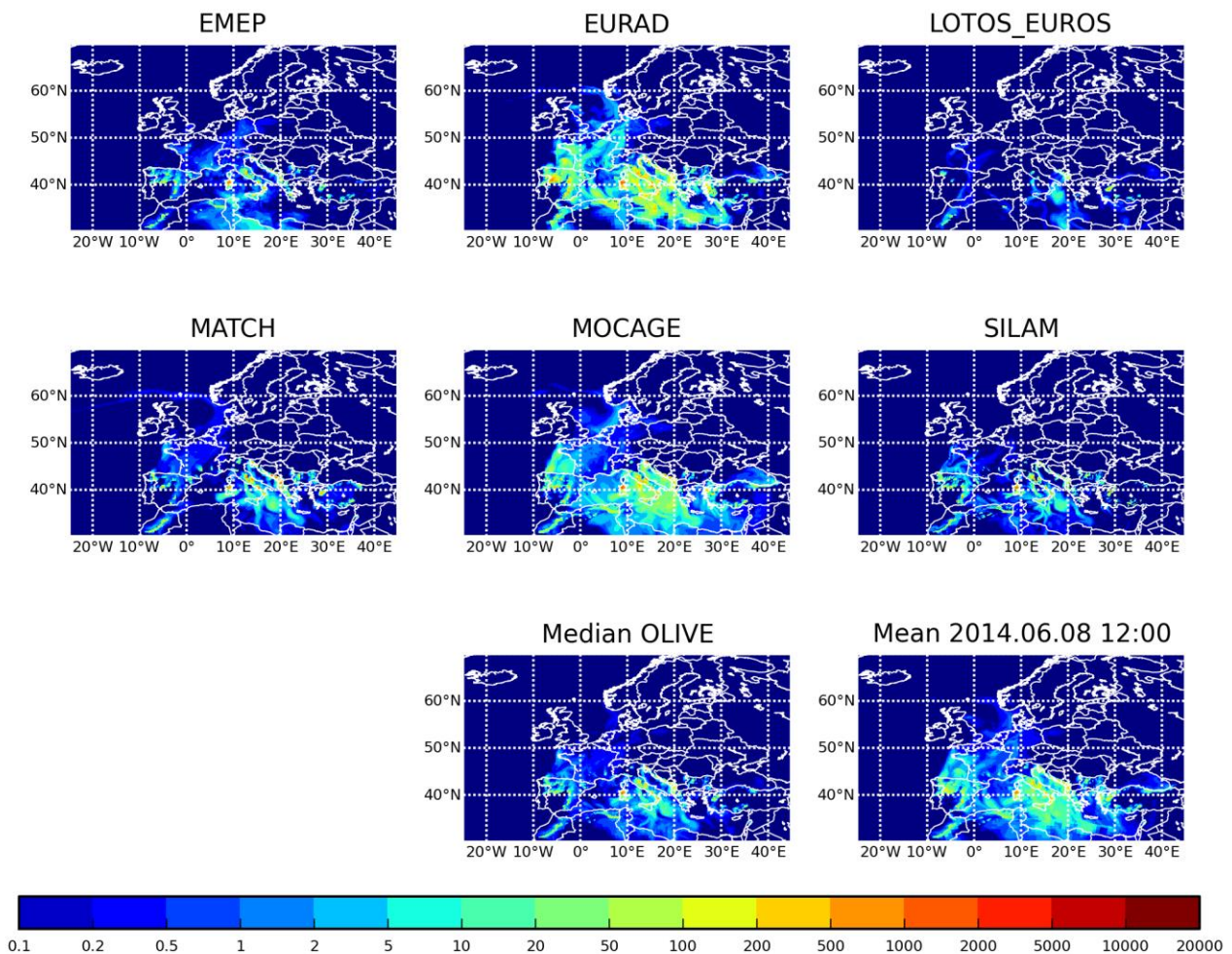
337

4.2. Model results

338 The total seasonal olive pollen load (Figure 3, Figure 4) expectedly correlates with the map of olive
339 plantations (Figure 1), which is also confirmed by the observations (Figure 3). The highest load is
340 predicted over Spain and Portugal, whereas the level in the Eastern Mediterranean is not so high
341 reflecting smaller size of the areas covered by the olive trees and limited long-range transport over
342 Mediterranean. The model predictions differ up to a factor of a few times (Figure 4), reflecting the
343 diversity of modelling approaches, especially the deposition and vertical diffusion
344 parameterizations (see Table 1 and section 3.1).

345 Since the olive plantations are located within a comparatively narrow climatic range, flowering
346 propagates through the whole region within a few weeks starting from the coastal bands and
347 progressing inland (not shown).

348



349

350

Figure 5. Example of hourly olive pollen concentrations, 12 UTC 08.06.2014, [pollen m^{-3}].

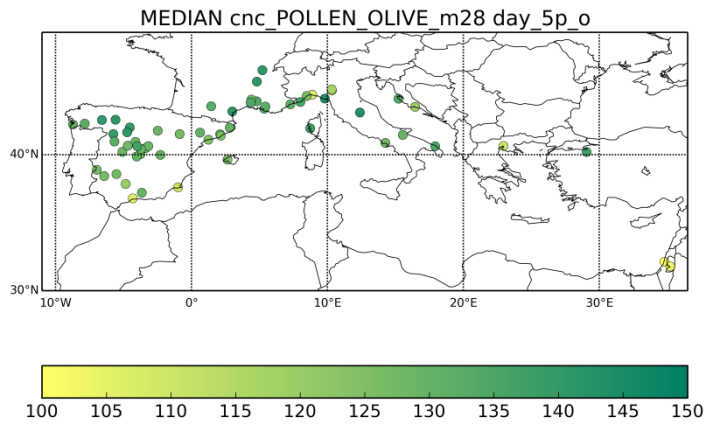
351

352 Hot weather during the flowering season leads to strong vertical mixing and deep atmospheric
353 boundary layer (ABL), which in turn promotes the pollen dispersion. As seen from Figure 5, the
354 pollen plumes can reach out over the whole Mediterranean and episodically affect Central Europe.
355 Both Figure 4 and Figure 5 illustrate the differences between the models, e.g. substantially higher
356 concentrations reported by EURAD-IM and MOCAGE as compared to other models. What regard
357 to pollen transport, the shortest transport with the fastest deposition is manifested by LOTOS-
358 EUROS (also, showed the lowest concentrations), while the longest one is suggested by MOCAGE.

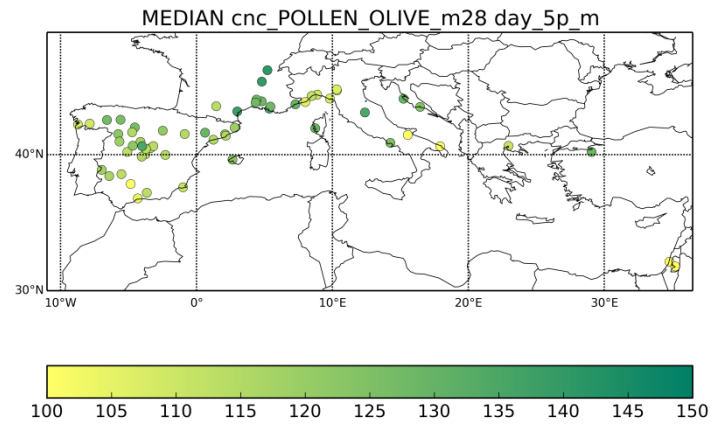
359 The most-important general parameters describing the season timing are its start and end (Figure 6).
360 Following Andersen (1991), these dates are computed as dates when 5% and 95% of the SPI are
361 reached.

362 Computations of the model-measurement comparison statistics faces the problem of non-
363 stationarity and non-normal distribution of the daily pollen concentrations (Ritenberga et al., 2016).
364 For such processes, usual non-parametric statistics have to be taken with high care since their basic
365 assumptions are violated. Nevertheless, they can be formally calculated for both individual models
366 and the ensemble (Figure 7, Figure 8). The main characteristic of the ensemble, the discrete rank
367 histogram and the distribution of the modelled values for the below-detection-limit observations
368 (Figure 9) show that the spread of the obtained ensemble is somewhat too narrow in comparison
369 with the dynamic range of the observations. The same limitation was noticed for the birch
370 ensemble.

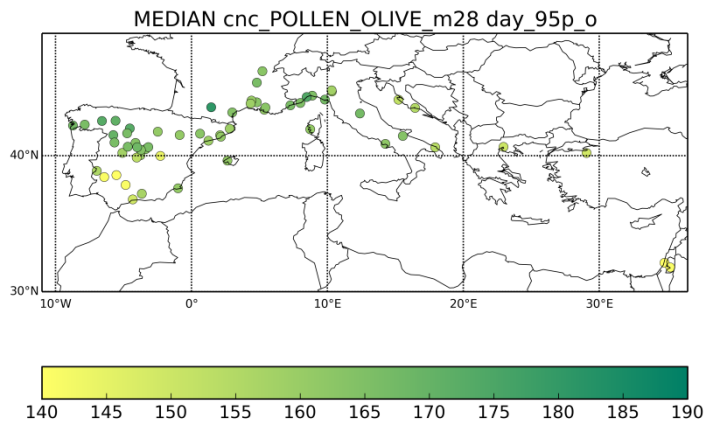
371 The patterns in Figure 6 and Figure 7 reveal a systematic early bias of the predicted season start and
372 end, which is well seen from normalised cumulative concentration time series (Figure 10). This bias
373 is nearly identical for all models, except for EURAD-IM, which also shows higher correlation
374 coefficient than other models. The reasons for the problem and for the diversity of the model
375 response are discussed in the next section.



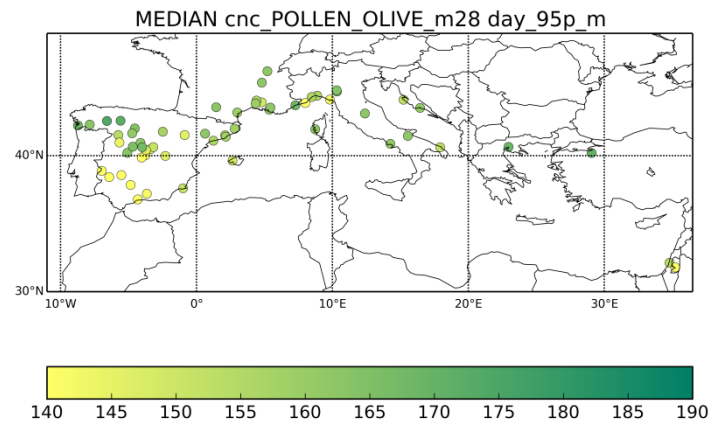
Season start day, 5%, observed



Season start day, 5%, ensemble median



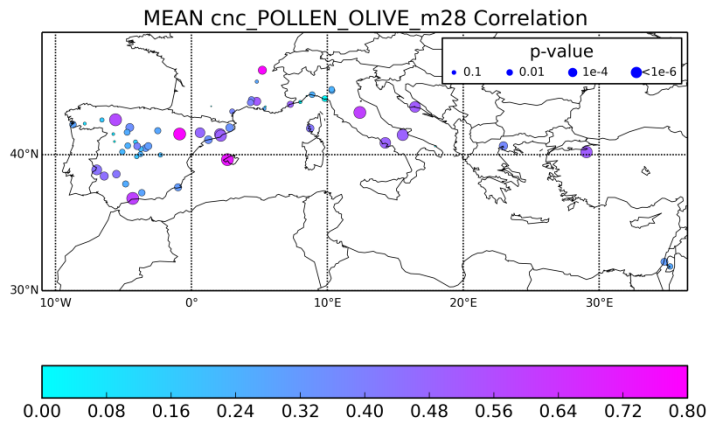
Season end day, 95%, observed



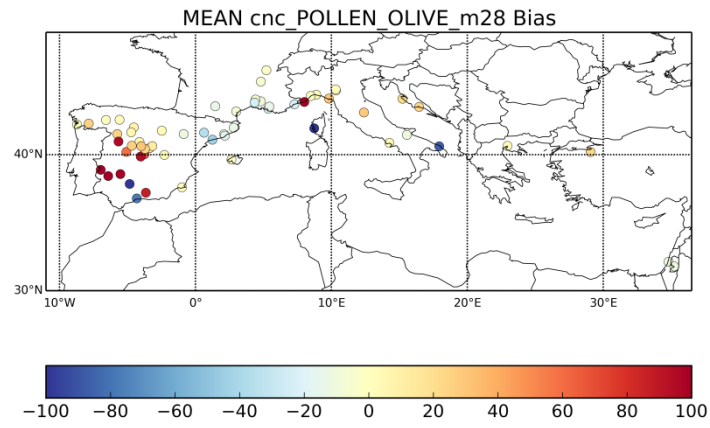
Season end day, 95%, ensemble median

376
377
378
379

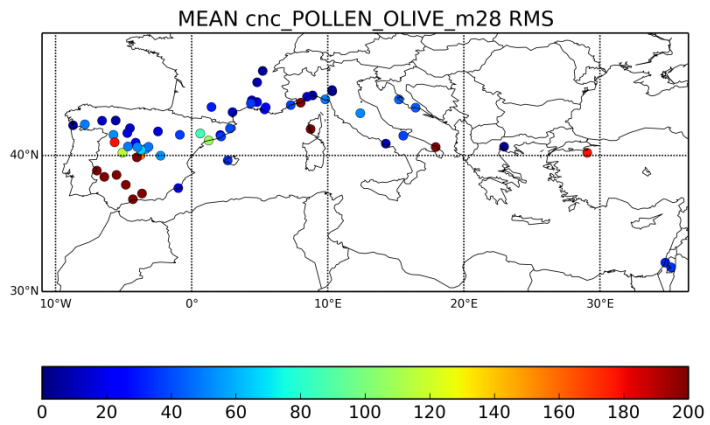
Figure 6. The start (date of 5% of the cumulative seasonal concentrations) and the end (95% of the cumulative seasonal concentrations) of the olive season in 2014 as day of the year, predicted by the median of the ensemble and observed by the stations with sufficient amount of observations.



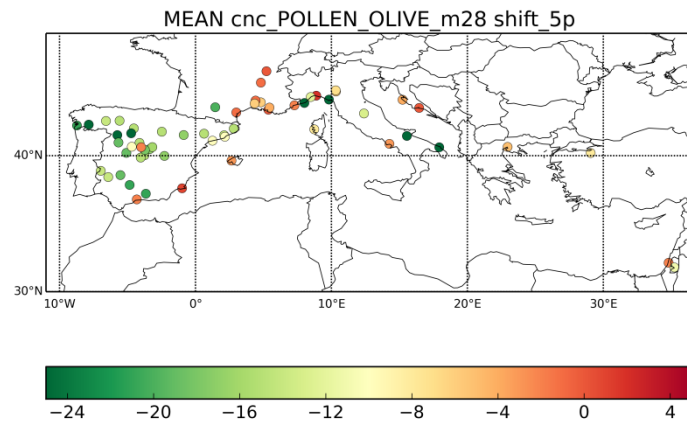
Correlation coefficient, dot size refers to p-value



Absolute bias, mean April-June, [pollen m⁻³]



RMSE, [pollen m⁻³]

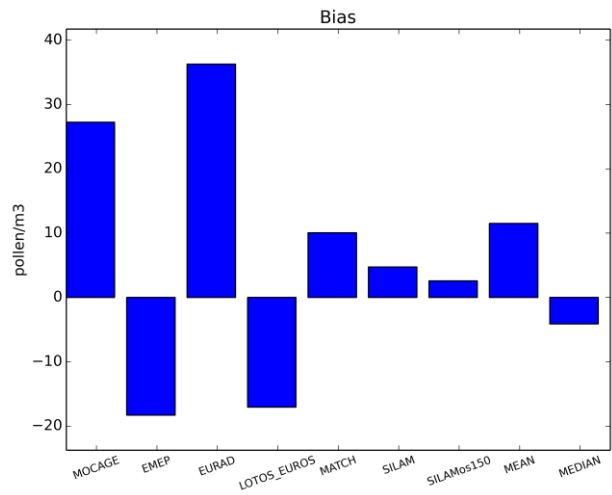
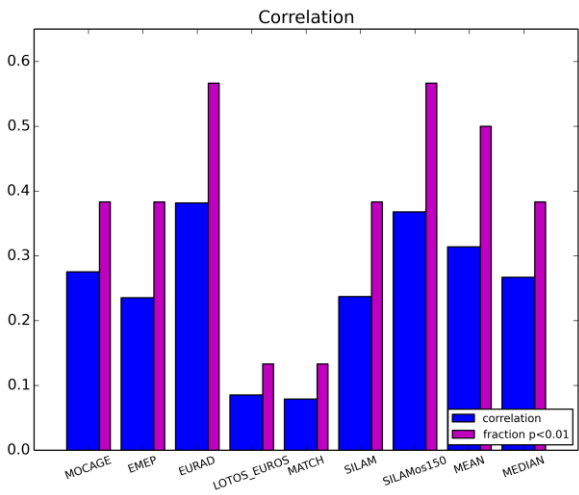


Error in the season start, days

380
381
382
383

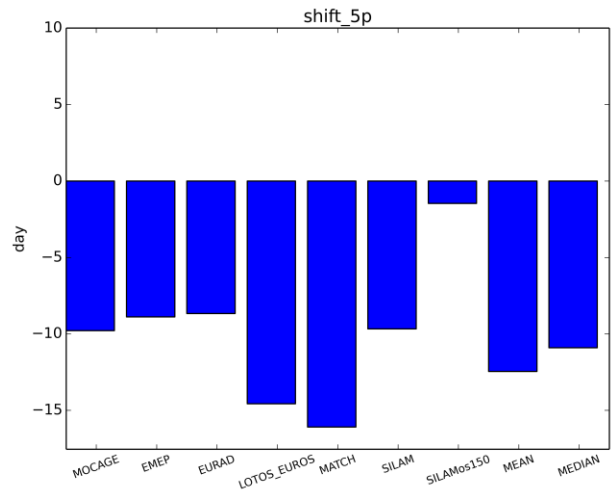
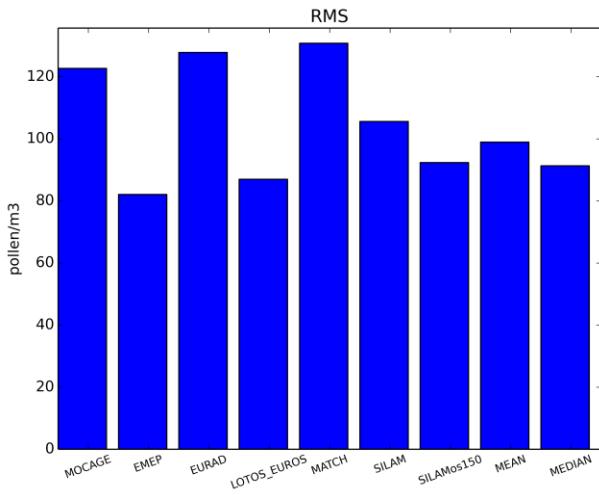
Figure 7. Results of model-measurement comparison for the ensemble mean: correlation coefficient for daily time series, mean bias April-June (pollen m⁻³), RMSE (pollen m⁻³), error in the season start (days).

384



Correlation coefficient and fraction of p < 0.01

Absolute bias, mean April-June [pollen m⁻³]



RMSE, [pollen m⁻³]

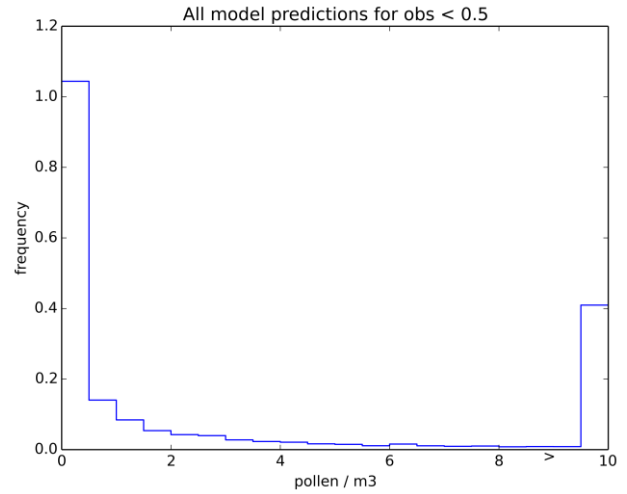
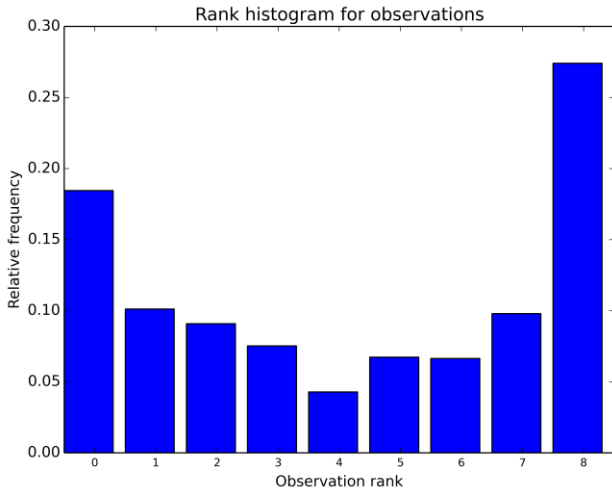
Error in the season start, days

385

386 **Figure 8.** Scores of the individual models, mean over all stations. The same parameters as in **Figure 7**. The sensitivity
387 run SILAMos150 is explained in the discussion section

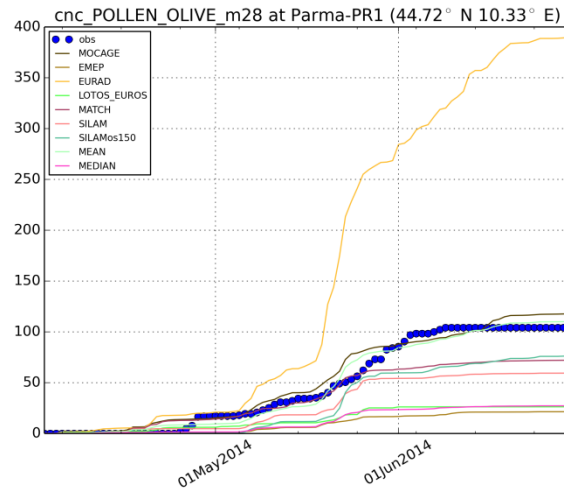
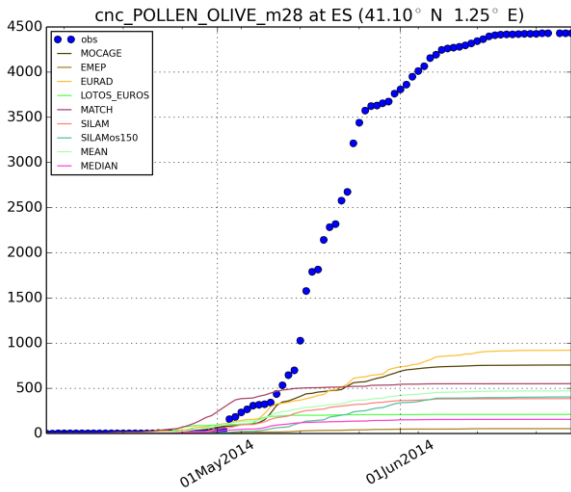
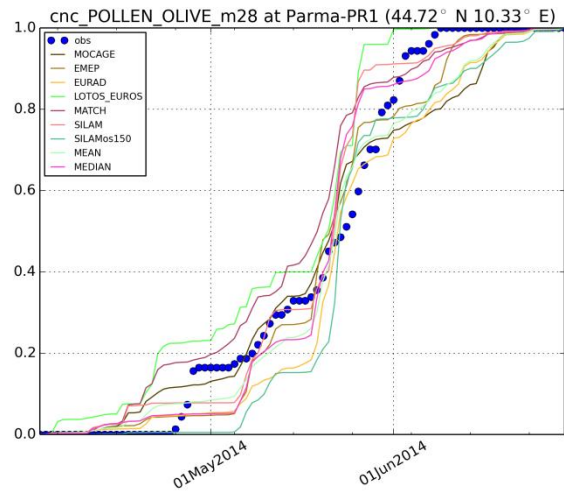
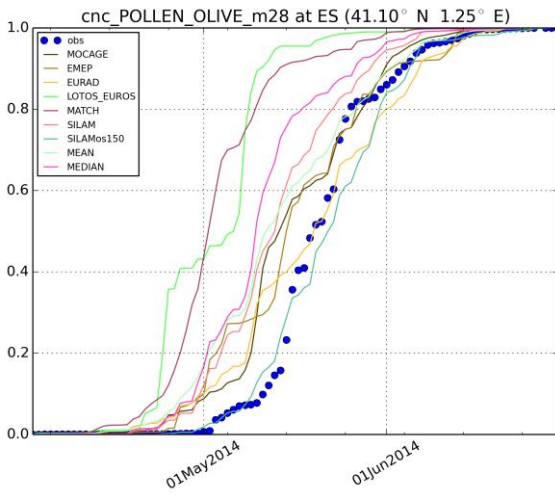
388

389



390
391
392
393

Figure 9. Ensemble characteristics. Left: discrete rank histogram for the constructed ensemble (daily concentration statistics); right: histogram of model predictions when observations were below the detection limit $0.5 \text{ pollen m}^{-3}$,



394
395
396

Figure 10. Cumulative time series of olive concentrations at Tarragona (Spain) and Parma (Italy). Upper row: normalized to the seasonal SPI [relative unit], lower: absolute cumulative concentrations [pollen day m^{-3}].

397 5. Discussion

398 In this section, we consider the key season parameters and the ability of the presented ensemble to
399 reproduce those (section 5.1), the added value of the multi-model ensembles, including the
400 optimized ensemble (section 5.2), main uncertainties that limit the model scores (section 5.3), and
401 the key challenges for future studies (section 5.4).

402 5.1. Forecast quality: model predictions for the key season parameters

403 The key date of the pollen season is its start: this very date refers to adaptation measures that need
404 to be taken by allergy sufferers. Predicting this date for olives is a significantly higher challenge
405 than, e.g., for birches: the heat sum has to be accumulated starting from 1 January with the season
406 onset being in mid-April, whereas for birches it is 1 March and mid-March, respectively. As a
407 result, prediction of the olive season start strongly depends on the temperature predictions by the
408 weather prediction model and the way this temperature is integrated into the heat sum.
409 Inconsistency between these, even if small, over the period of almost 4 months can easily lead to a
410 week of an error. As one can see from Figure 8 and Figure 7, there is a systematic, albeit spatially
411 inhomogeneous bias of all models by up to 10 days (too early season). Exception is the
412 SILAMos150 sensitivity run, which used the higher heat sum threshold, by 150 degree-days
413 (~10%), than the standard level (Figure 2). No other sensitivity runs, including the simulations
414 driven by ERA-Interim fields, showed any significant improvement of this parameter. Importantly,
415 EURAD-IM, which is driven by WRF meteo fields, also showed a similar bias. Finally, the shift
416 varies among the stations: from near-zero (France, some sites in Italy, Croatia, Greece, and Israel)
417 up to almost three weeks in North-Western Spain. It means that no “easy” solution exists and calls
418 for an analysis of long-term time series, aiming at refinement of the heat sum formulations and
419 threshold values.

420 The end of the season showed an intriguing picture: EURAD-IM, despite starting the season as
421 early as all other models, ends it 2 days too late instead of 5 days too early as all other models (see
422 examples for two stations in Figure 10). This indicates that WRF, in late spring, predicts lower
423 temperature than IFS, which leads to longer-than-observed season in the EURAD-IM predictions.
424 Other models showed correct season length and, due to initial early bias, end it a few days too early.
425 The de-biased run SILAMos150 run shows almost perfect shape and hits both start and end with 1
426 day accuracy, which supports 250 degree day as a season length parameter.

427 The most-diverged model predictions are shown for the absolute concentrations (Figure 8). With the
428 mean observed April-June concentration of 35 pollen m⁻³ the range of predictions spans over a
429 factor of four: EURAD-IM and MOCAGE being twice higher and EMEP and LOTOS-EUROS
430 twice lower. Shifting the season by 5 days in the SILAMos150 run also changes the model bias,
431 reflecting differences in the transport patterns and the impact of stronger vertical mixing in later
432 spring. Spatially, the bias is quite homogeneous, except for southern Spain, where heterogeneous
433 pattern is controlled by local conditions at each specific site (Figure 7).

434 Temporal correlation is generally high in coastal areas (Figure 7) but at or below 0.5 in terrestrial
435 stations of Iberian Peninsula (the main olive plantations). This is primarily caused by the shifted
436 season: the simulations with more accurate season showed the highest correlation among all models
437 with ~60% of sites with significant correlation (p<0.01, Figure 8).

438 Comparison with local statistical models made for single or a few closely-located stations
439 expectedly shows that local models are usually comparable but somewhat more accurate (at their
440 locations) than the European-scale dispersion models (see also discussion in (Ritenberga et al.,
441 2016)). Thus, (Gala et al., 2001) analyzed performance of three popular local models for Cordoba,
442 with the best one showing the mean error of the start of the season of 4.7 days but reaching up to 14
443 days in some years. Similar error was found for Andalusia (Galán et al., 2005) and two sites
444 (Perugia and Ascoli Piceno) in Italy (Frenguelli et al., 1979) – 4.8 and 4.33 days of the standard
445 error, respectively. A recent study (Aguilera et al., 2014) constructed three independent statistical
446 models for Spain, Italy and Tunisia and ended up with over 5 days of a standard error for the
447 Mediterranean. In another study, the authors admitted the scale of the challenges: “The specific
448 moment for the onset of the olive heat accumulation period is difficult to determine and has
449 essentially remained unknown” (Aguilera et al., 2013).

450 One of the strengths of continental-scale dispersion models is their ability to predict long-range
451 transport events. However, direct evaluation of this feature for olive pollen is difficult since
452 countries without olive plantations usually do not count its pollen. One can however refer to Figure
453 3 (zoomed map of Spain), which shows that the ensemble successfully reproduces the drastic
454 change of the SPI from nearly 10⁵ pollen day m⁻³ in the south of Spain down to less than 100 pollen
455 day m⁻³ in the north. Episode-wise, an example of a well-articulated case of olive pollen transport
456 from Italy to Hungary in 2016 was brought up by Udvardy et al., (2017), who analyzed it with
457 adjoint SILAM simulations. The episode was also well-predicted by the forward computations.

458 5.2. Ensemble added value

459 Arguably the main uncertainty of the model predictions was caused by the shift of the season start
460 and end – the parameters heavily controlled by temperature, i.e. least affected by transport features
461 of the models. As a result, application of the “simple” ensemble technologies does not lead to a
462 strong improvement. Some effect was still noticed but less significant than in case of birch or
463 traditional AQ forecasting. Therefore, in this section we also consider a possibility of ensemble-
464 based fusion of the observational data with the model predictions. All ensembles were based on
465 operational models, i.e. the SILAMos150 run was not included in either of them.

466 5.2.1. Mean ensembles: arithmetic average and median

467 Considering the mean-ensemble statistics, one should keep in mind that both the meteorological
468 driver and the source term parameterization were the same for all models (except for EURAD
469 driven by WRF). This resulted in the under-representative ensemble (Figure 9), where several good
470 and bad features visible in all models propagate to the mean ensembles.

471 Among the simple means, arithmetic average performed better than the median, largely owing to
472 strong EURAD-IM impact. That model over-estimated the concentrations and introduced a
473 powerful push towards extended season, thus offsetting the early bias of the other models. Since
474 median largely ignored this push, its performance was closer to that of other models. Nevertheless,
475 both mean and median demonstrated low RMSE, median being marginally better.

476 5.2.2. Fusing the model predictions and observations into an optimized 477 ensemble: gain in the analysis and predictive capacity

478 Developing further the ensemble technology, we present here the first attempt of fusion of the
479 observational data with the multi-model ensemble for olive pollen.

480 In the Section 3.1, the Eq. (2) requires three parameters to prescribe: the regularization scaling
481 parameters α and β , and length of the assimilation window T . For the purposes of the current
482 feasibility study, several values for each of the parameters were tested and the robust performance
483 of the ensemble was confirmed with very modest regularization strength and for all considered
484 lengths of the analysis window – from 1 to 15 days. Finally, $\alpha = 0.1$, $\beta = 0.1$, $T = 5 \text{ days}$ were
485 selected for the below example as a compromise between the smoothness of the coefficients,
486 regularization strength and the optimization efficiency over the assimilation window.

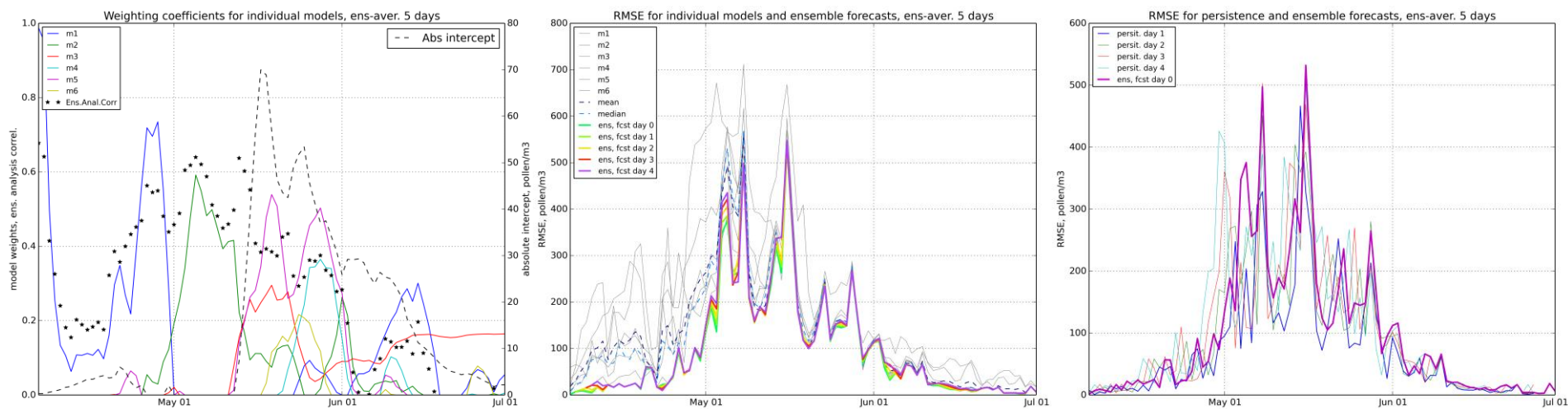
487 The optimized ensemble showed (Figure 11, left-hand panel) that each of the 6 models had
488 substantial contribution over certain parts of the period. Over some times, e.g. during the first half
489 of May, only one or two models were used, other coefficients being put to zero, whereas closer to
490 the end of the month, all models were involved. Finally, prior to and after the main season,
491 concentrations were very low and noisy, so the regularization terms of Eq. (2) took over and pushed
492 the weights to a-priori value of $1/6$.

493 The bulk of the improvements came in the first half of the season (Figure 11, middle panel). After
494 the third peak in the middle of May, the effect of assimilation becomes small and the optimization
495 tends to use intercept to meet the mean value, whereas the model predictions become small and
496 essentially uncorrelated with the observations. This corroborates with the observed 8-days shift of
497 the season, which fades out faster in the models than in the observed time series (Figure 10).

498 There was little reduction of the predictive capacity of the optimized ensemble when going out of
499 assimilation window towards the forecasts. In-essence, only the first peak of concentrations (and
500 RMSE) is better off with shorter forecasts. For the rest of the season (before and after the peak) the
501 5-day assimilation window led to a robust combination of the models that stayed nearly-optimal
502 over the next five days.

503 Comparison with other forecasts expectedly shows that the optimized ensemble not only has
504 significantly better skills than any of the individual models, but is up to 25-30% better than mean
505 and median of the ensemble (Figure 11, middle panel). A stronger competitor was the “persistence
506 forecast” when the next-day(s) concentrations are predicted to be equal the last observed daily
507 value. The one-day persistence appeared to be the best-possible “forecast”, which shows at the
508 beginning of May almost twice lower RMSE than the one-day forecast of the optimal ensemble
509 (Figure 11, right-hand panel). However, already two-days persistence forecast had about-same
510 RMSE as the ensemble, and 3- and 4- days predictions were poor.

511



512

513 **Figure 11.** Optimal weights of the individual models and ensemble correlation score over the 5-days-long assimilation window (left panel); RMSE of the of individual models
514 and the optimal ensemble forecasts against those of individual models and simple ensemble means (middle) and against persistence-based forecasts (right-hand panel).

515

516 Strong performance of the one-day persistence forecast is not surprising and, with the current
517 standards of the pollen observations, has no practical value: the data are always late by more than
518 one day (counting can start only next morning and become available about mid-day). The second
519 problem of the persistence forecast is that it needs actual data, i.e. the scarcity of pollen network
520 limits its coverage. Thirdly, persistence loses its skills very fast: already day+2 forecast has no
521 superiority to the optimal ensemble, whereas day+3 and +4 persistence-based predictions are
522 useless. Finally, at local scale, state-of-art statistical models can outperform it – see discussion in
523 (Ritenberga et al., 2016).

524 One should however point out that one-day predicting power of the persistence forecast (or more
525 sophisticated statistical models based on it) can be a strong argument for the future real-time online
526 pollen monitoring, which delay can be as short as one hour (Crouzy et al., 2016; Oteros et al.,
527 2015). Such data have good potential as the next-day predictions for the vicinity of the monitor.

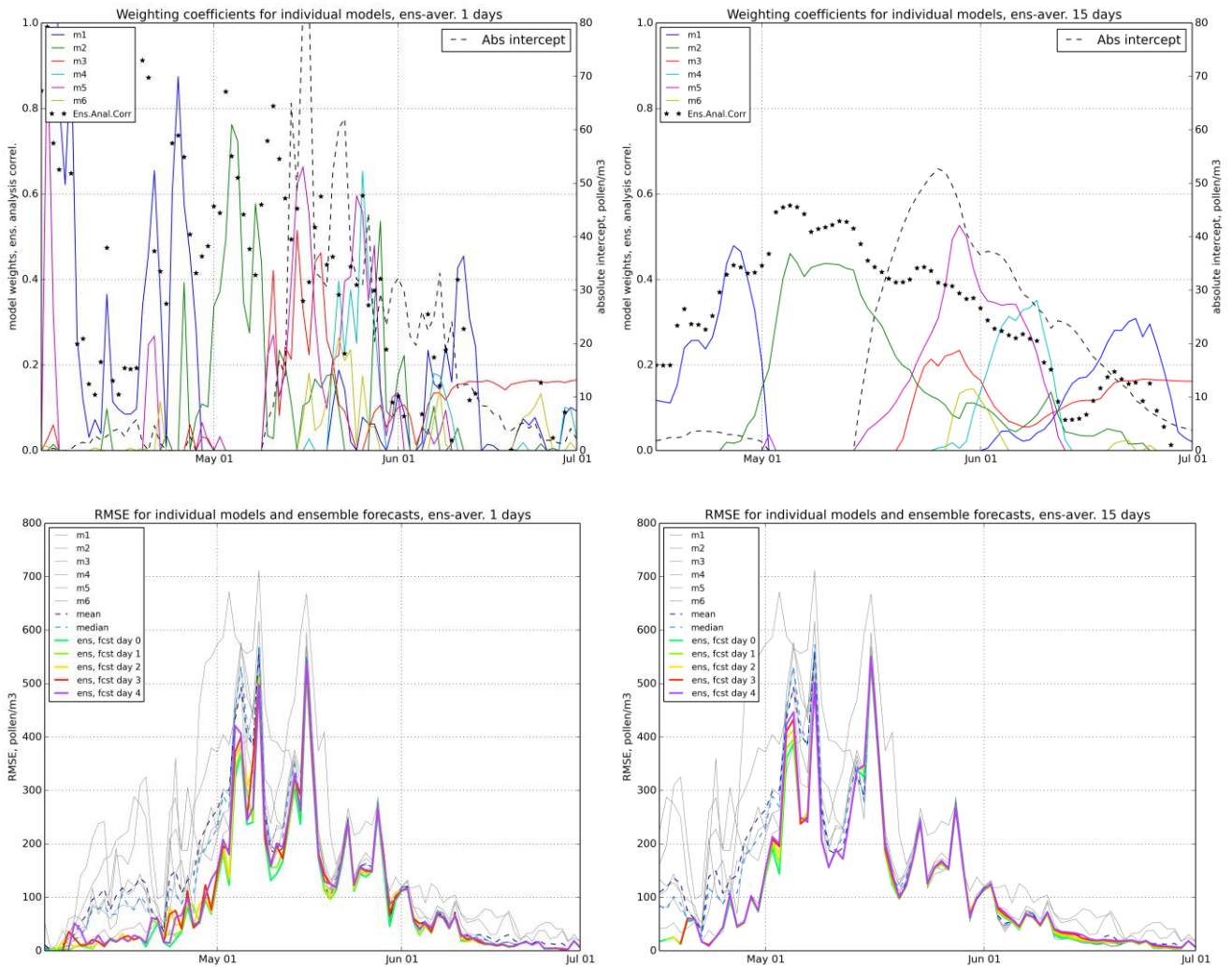
528 5.3.Sensitivity of the simulations to model and source term parameters

529 The above-presented results show that arguably the most-significant uncertainty was due to shifting
530 the start and the end of the season. It originated from the long heat sum accumulation (since 1
531 January), where even a small systematic difference between the meteorology driving the multi-
532 annual fitting simulations and that used for operational forecasts integrates to a significant season
533 shift by late spring. In some areas, resolution of NWP model plays as well: complex terrain in the
534 north of Spain and in Italy requires dense grids to resolve the valleys. Other possible sources of
535 uncertainties might need attention.

536 To understand the importance of some key parameters, a series of perturbed runs of SILAM was
537 made:

- 538 - **os100** and **os150** runs with the season starting threshold increased by 100 and 150 degree
539 days (the **os150** run is referred in the above discussion as SILAMos150)
- 540 - **era** run with ERA-Interim meteorological fields, which were used for the source parameters
541 fitting
- 542 - series of 3 runs with reduced vertical mixing within the ABL and the free troposphere
- 543 - **smlpoll** run with 20 µm size of the pollen grain
- 544 - **smlpoll_coarse** run with 20 µm pollen size and coarse computational grid (0.2°×0.2°)

545



546

547 **Figure 12.** Sensitivity of optimized ensemble to the length of assimilation window. Upper row: optimal weights of the
 548 individual models and ensemble score over the 1- (left) and 15- (right) days-long assimilation windows; lower row:
 549 RMSE of the of individual models and the optimal ensemble forecasts against those of individual models. Obs. earlier
 550 first available date for 1-day-analysis window.

551

552 The **era** simulations with ERA-Interim reduced the shift of the season start by 2 days but increased
 553 the shift of the end by 3 days, i.e. made the season shorter by 5 days. At the same time, the **os150**
 554 run showed that a simple increase of the heat sum threshold by ~10% (150 degree days) essentially
 555 eliminates the mean shift – for 2014 – but it remains unclear whether this adjustment is valid for
 556 other years.

557 Variations of the mixing parameterization (perturbing the formula for the K_z eddy diffusivity) did
 558 not lead to significant changes: all scores stayed within 10% of the reference SILAM simulations.

559 Evaluation of the impact of deposition parameterizations was more difficult since they are model-
560 specific. Higher deposition intensity causes both reduction of the transport distance and absolute
561 concentrations. This issue might be behind the low values reported by LOTOS-EUROS and,
562 conversely, high concentrations of EURAD-IM and MOCAGE. Its importance was confirmed by
563 the SILAM sensitivity simulations with smaller pollen size, **smlpoll** and **smlpoll_coarse**. Both runs
564 resulted in more than doubling the mean concentrations but with marginal effect on temporal
565 correlation. They also differed little from each other.

566 Variations of the fusion parameters showed certain effect. For short averaging window (5 days or
567 less), the variations of weighting coefficients increased and the time series became noisier (Figure
568 12). On return, the correlation increased almost up to 0.8 – 0.9 for some analysis intervals, though
569 stayed the same for other periods. Also, the one-day forecast RMSE decreased for some days but
570 little difference was found for longer predictions.

571 5.4. Main challenges for the future studies

572 The current study is the first application of numerical models to olive pollen dispersion in Europe.
573 One of its objectives was to identify the most-pressing limitations of the current approach and the
574 extent to which the ensemble and data fusion technologies can help in improving the forecasts.

575 The most-evident issue highlighted by the exercise is the shift of the pollen season in some key
576 regions, which is similar in all models suggesting some unresolved inconsistencies between the
577 heat-sum calculations of the source term and the features of the temperature predictions by the
578 weather model. The issue suggests some factor(s) currently not included or mis-interpreted in the
579 source term. One of the candidate processes is the chilling-sum accumulation suggested by some
580 studies, e.g., (Aguilera et al., 2014). A switch to different types of phenological models with genetic
581 differentiation of the populations following Chuine and Belmonte, (2004) is another promising
582 option.

583 The second issue refers to the under-estimation of the pollen concentration in France, which
584 probably originates from a comparatively large number of olive trees spread in private gardens etc
585 but not accounted for in the agriculture maps of olive plantations.

586 The third set of questions refers to the pollen load prediction, i.e. a possibility to forecast the overall
587 season severity before it starts. Several statistical models have been presented in the literature, e.g.,
588 (Ben Dhiab et al., 2016) for total annual load and (Chuine and Belmonte, 2004) for relative load.
589 Their evaluation and implementation in the context of dispersion models is important.

590 An issue, mostly addressing the long-term horizon rather than the short-term forecasts is the validity
591 of the developed models in the conditions of changing climate. The models have to be robust to the
592 trends in meteorological forcing. Purely statistical models are among the most vulnerable in this
593 respect because they just quantify the apparent correlations observed under certain conditions but
594 do not explore the processes behind these relations.

595 Finally, already the first steps towards ensemble-based fusion of the model forecasts and pollen
596 observations showed strong positive effect. Further development of these techniques combined with
597 progress towards near-real-time pollen data has very high potential for improving the forecasts.

598

599 6. Summary

600 An ensemble of 6 CAMS models was run through the olive flowering season of 2014 and compared
601 with observational data of 8 countries of European Aeroallergen Network (EAN).

602 The simulations showed decent level of reproduction of the short-term phenomena but also
603 demonstrated a shift of the whole season by about 8 days (~20% of the overall pollination period).
604 An ad-hoc adjustment of the season-start heat sum threshold by ~10% (150 degree days) in-average
605 resolves the issue and strongly improves the model skills but its regional features and validity for
606 other years and meteorological drivers remain unclear.

607 The ensemble members showed quite diverse pictures demonstrating the substantial variability,
608 especially in areas remote from the main olive plantations. Nevertheless, the observation rank
609 histogram still suggested certain under-statement of the ensemble variability in comparison with the
610 observations. This partly originates from the synchronized source term formulations and
611 meteorological input used by all but one models.

612 Simple ensemble treatments, such as arithmetic average and median, resulted in a more robust
613 performance but they did not outrun the best models over significant parts of the season. Arithmetic
614 average turned out to be better than median.

615 A data-fusion approach, which creates the optimal-ensemble model using the observations over
616 preceding days for optimal combination of the ensemble members, is suggested and evaluated. It
617 was based on an optimal linear combination of the individual ensemble members and showed strong
618 skills, routinely outperforming all individual models and simple ensemble approaches. It also
619 showed strong forecasting skills, which allowed application of the past-time model weighting

620 coefficients over several days in the future. The only approach outperforming this fusion ensemble
621 was the one-day persistence-based forecast, which has no practical value due to the manual pollen
622 observations and limited network density. It can however be used in the future when reliable online
623 pollen observations will become available.

624 A series of sensitivity simulations highlighted the importance of meteorological driver, especially
625 its temperature representation, and deposition mechanisms. The data fusion procedure was quite
626 robust with regard to analysis window, still requiring 5-7 days for eliminating the noise in the
627 model weighting coefficients.

628

629 7. Acknowledgements

630 The work was performed within the scope of Copernicus Atmospheric Monitoring Service CAMS,
631 funded by the European Union's Copernicus Programme. Support by performance-based funding of
632 University of Latvia is also acknowledged. Observational data were provided by national pollen
633 monitoring of Croatia, Greece, France, Italy (A.I.A.-R.I.M.A.[®]), Spain (REA: Aerocam, AeroUEx,
634 RAA, UO, UC and Cantabria Health Council, REDAEROCAM, Health Castilla-Leon Council,
635 RACyL, XAC, RIAG, PalinoCAM, UPCT, Basque Government / Public Health Directory),
636 Hungary, Israel, and Turkey, members of the European Aeroallergen Network EAN. The olive
637 source term is a joint development of Finnish Meteorological Institute and EAN research teams,
638 created within the scope of the Academy of Finland APTA project. This work contributes to the
639 ICTA 'Unit of Excellence' (MinECo, MDM2015-0552).

640 The material is published in the name of the European Commission; the Commission is not
641 responsible for any use that may be made of the information/material contained.

642

643 8. References

644 Aguilera, F., Ben Dhiab, A., Msallem, M., Orlandi, F., Bonofiglio, T., Ruiz-Valenzuela, L., Galán,
645 C., Díaz-de la Guardia, C., Giannelli, A., Trigo, M.M., García-Mozo, H., Pérez-, Badia, R.,
646 Fornaciari, M., 2015. Airborne-pollen maps for olive-growing areas throughout the
647 Mediterranean region: spatio-temporal interpretation. *Aerobiologia* (Bologna). 31, 421–434.

648 Aguilera, F., Fornaciari, M., Ruiz-Valenzuela, L., Galán, C., Msallem, M., Dhiab, A. Ben, la
649 Guardia, C.D. de, del Mar Trigo, M., Bonofiglio, T., Orlandi, F., 2014. Phenological models to
650 predict the main flowering phases of olive (*Olea europaea* L.) along a latitudinal and

- 651 longitudinal gradient across the Mediterranean region. *Int. J. Biometeorol.* 59, 629–641.
652 doi:10.1007/s00484-014-0876-7
- 653 Aguilera, F., Ruiz, L., Fornaciari, M., Romano, B., Galán, C., Oteros, J., Ben Dhiab, A., Msallem,
654 M., Orlandi, F., 2013. Heat accumulation period in the Mediterranean region: phenological
655 response of the olive in different climate areas (Spain, Italy and Tunisia). *Int. J. Biometeorol.*
656 58, 867–876.
- 657 Alba, F., Di?az De La Guardia, C., 1998. The effect of air temperature on the starting dates of the
658 *Ulmus*, *Platanus* and *Olea* pollen seasons in the SE Iberian Peninsula. *Aerobiologia* (Bologna).
659 14, 191–194.
- 660 Andersen, T.B., 1991. A model to predict the beginning of the pollen season. *Grana* 30, 269–275.
661 doi:10.1080/00173139109427810
- 662 Baklanov, A., Sorensen, J.H., 2001. Parameterisation of radionuclide deposition in atmospheric
663 long-range transport modelling. *Phys. Chem. Earth, Parts B* 26, 787–799.
- 664 Barranco, D., Fernández-Escobar, R., Rallo, L., 2008. *El Cultivo del olivo* (8^a Ed). Madrid.
- 665 Bechtold, P., Bazile, E., Guichard, F., Mascart, P., Richard, E., 2001. A mass-flux convection
666 scheme for regional and global models. *Quarterly J. R. Meteorol. Soc.* 127, 869–886.
- 667 Ben Dhiab, A., Ben Mimoun, M., Oteros, J., Garcia-Mozo, H., Domínguez-Vilches, E., Galán, C.,
668 Abichou, M., Msallem, M., 2016. Modeling olive-crop forecasting in Tunisia. *Theor. Appl.*
669 *Climatol.* 1–9. doi:10.1007/s00704-015-1726-1
- 670 Bott, A., 1989. A positive definite advection scheme obtained by nonlinear renormalization of the
671 advective fluxes. *Mon. Weather Rev.* 117, 1006–1016.
- 672 Cebrino, J., Portero de la Cruz, S., Barasona, M.J., Alcázar, P., Moreno, C., Domínguez-Vilches, E.,
673 Galán, C., 2017. Airborne pollen in Córdoba City (Spain) and its implications for pollen
674 allergy. *Aerobiologia* (Bologna). 33, 281–291. doi:10.1007/s10453-016-9469-8
- 675 CEC, 1993. *CORINE Land Cover Technical Guide*. Luxembourg.
- 676 Champeaux, J.L., Masson, V., Chauvin, F., 2005. ECOCLIMAP: a global database of land surface
677 parameters at 1 km resolution. *Meteorol. Appl.* 29–32.
- 678 Chuine, I., Belmonte, J., 2004. Improving prophylaxis for pollen allergies : Predicting the time
679 course of the pollen load of the atmosphere of major allergenic plants in France and Spain.
680 *Grana* 43, 65–80. doi:10.1080/00173130410019163
- 681 Crouzy, B., Stella, M., Konzelmann, T., Calpini, B., Clot, B., 2016. All-optical automatic pollen
682 identification: Towards an operational system. *Atmos. Environ.* 140, 202–212.
683 doi:10.1016/j.atmosenv.2016.05.062
- 684 D’Amato, G., Cecchi, L., Bonini, S., Nunes, C., Annesi-Maesano, I., Behrendt, H., Liccardi, G.,
685 Popov, T., van Cauwenberge, P., 2007. Allergenic pollen and pollen allergy in Europe. *Allergy*
686 62, 976–990. doi:10.1111/j.1398-9995.2007.01393.x
- 687 D’Amato, G., Cecchi, L., Bonini, S., Nunes, C., Annesi-Maesano, I., Behrendt, H., Liccardi, G.,
688 Popov, T., van Cauwenberge, P., 2007. Allergenic pollen and pollen allergy in Europe. *Allergy*
689 62, 976–990.
- 690 de Weger, L., Bergmann, K.-C., Rantio-Lehtimäki, A., Dahl, Å., Buters, J.T.M., Dechamp, C.,
691 Belmonte, J., Thibaudon, M., Cecchi, L., Besancenot, J.-P., Gala, C., Waisel, Y., 2013. Impact
692 of pollen, in: Sofiev, M., Bergmann, K.-C. (Eds.), *Allergenic Pollen. A Review of the*

- 693 Production, Release, Distribution and Health Impacts. Springer Netherlands, Dordrecht, p. x +
694 247. doi:10.1007/978-94007-4881-1
- 695 Elbern, H., Strunk, A., Schmidt, H., Talagrand, O., 2007. Emission rate and chemical state
696 estimation by 4-dimensional variational inversion. *Atmos. Chem. Phys.* 7, 3749–3769.
- 697 Fernandez-Escobar, R., Benlloch, M., Navarro, C., G.C., M., 1992. The Time of Floral Induction in
698 the Olive. *J. Am. Soc. Hortic. Sci.* 117, 304–307.
- 699 Fornaciari, M., Pieroni, L., Ciuchi, P., Romano, B., 1998. A regression model for the start of the
700 pollen season in *Olea europaea*. *Grana* 37, 110–113.
- 701 Frenguelli, G., Bricchi, E., Romano, B., Mincigrucci, G., Spiexsma, F.T.M., 1979. A predictive
702 study on the beginning of the pollen season for Gramineae and *Olea europaea* L .
703 *Aerobiologia* (Bologna). 5, 64–70.
- 704 Gala, C., Garcia-Mozo, H., Carinanos, P., Alcazar, P., Dominguez-Vilches, E., 2001. The role of
705 temperature in the onset of the *Olea europaea* L. pollen season in southwestern Spain. *Int. J.*
706 *Biometeorol.* 45, 8–12.
- 707 Galan, C., Alcazar, P., Oteros, J., Garcia-Mozo, H., Aira, M.J., Belmonte, J., Diaz de la Guardia, C.,
708 Fernandez-Gonzalez, D., Gutierrez-Bustillo, M., Moreno-Grau, S., Perez-Badia, R.,
709 Rodriguez-Rajo, J., Ruiz-Valenzuela, L., Tormo, R., Trigo, M.M., Dominguez-Vilches, E.,
710 2016. Airborne pollen trends in the Iberian Peninsula. *Sci. Total Environ.* 550, 53–59.
711 doi:10.1016/j.scitotenv.2016.01.069
- 712 Galan, C., Antunes, C., Brandao, R., Torres, C., Garcia-Mozo, H., Caeiro, E., Ferro, R., Prank, M.,
713 Sofiev, M., Albertini, R., Berger, U., Cecchi, L., Celenk, S., Grewling, L., Jackowiak, B.,
714 J?ger, S., Kennedy, R., Rantio-Lehtim?ki, A., Reese, G., Sauliene, I., Smith, M., Thibaudon,
715 M., Weber, B., Weichenmeier, I., Pusch, G., Buters, J.T.M., 2013. Airborne olive pollen
716 counts are not representative of exposure to the major olive allergen *Ole e 1*. *Allergy Eur. J.*
717 *Allergy Clin. Immunol.* 68. doi:10.1111/all.12144
- 718 Galán, C., García-Mozo, H., Vázquez, L., Ruiz, L., De La Guardia, C.D., Trigo, M., 2005. Heat
719 requirement for the onset of the *Olea europaea* L. pollen season in several sites in Andalusia
720 and the effect of the expected future climate change. *Int. J. Biometeorol.* 49, 184–188.
- 721 Galán, C., Smith, M., Thibaudon, M., Frenguelli, G., Oteros, J., Gehrig, R., Berger, U., Clot, B.,
722 Brandao, R., Group, E.Q.W., 2014. Pollen monitoring: minimum requirements and
723 reproducibility of analysis. *Aerobiologia* (Bologna). 30, 385–395.
- 724 García-mozo, H., Galán, C., Jato, V., Belmonte, J., Díaz, C., Guardia, D., Fernández, D., Aira, M.J.,
725 Roure, J.M., Ruiz, L., Trigo, M.M., Domínguez-vilches, E., 2006. *Quercus* pollen season
726 dynamics in the Iberian Peninsula: response to meteorological parameters and posible
727 consequences of climate change. *Ann. Agric. Environ. Med.* 209–224.
- 728 Garcia-Mozo, H., Yaezel, L., Oteros, J., Galan, C., 2014. Statistical approach to the analysis of
729 olive long-term pollen season trends in southern Spain. *Sci. Total Environ.* 473–474, 103–109.
730 doi:10.1016/j.scitotenv.2013.11.142
- 731 Genikhovich, E., Pavlova, T. V, Kattsov, V.M., 2010. On complexing the ensemble of climate
732 models (In Russian: O kompleksirovanii ansamblya klimaticheskih modelej). *Proc. Voeikov*
733 *Main Geophysical Obs.* 7, 28–46.
- 734 Giorgi, F., Chameides, W.L., 1986. Rainout lifetimes of highly soluble aerosols and gases as
735 inferred from simulations with a general circulation model. *J. Geophys. Res.* 91, 14367–14376.

- 736 Gioulekas, D., Papakosta, D., Damialis, A., Spieksma, F.T.M., Giouleka, P., Patakas, D., 2004.
737 Allergenic pollen records (15 years) and sensitization in patients with respiratory allergy in
738 Thessaloniki , Greece. *Allergy* 174–184.
- 739 Gómez, J.A., Infante-Amate, J., González de Molina, M., Vanwalleghem, T., Taguas, E.V., Lorite,
740 I., 2014. Olive Cultivation, its Impact on Soil Erosion and its Progression into Yield Impacts in
741 Southern Spain in the Past as a Key to a Future of Increasing Climate Uncertainty. *Agriculture*
742 4, 170–198. doi:10.3390/agriculture4020170
- 743 Hass, H., Jakobs, H.J., Memmesheimer, M., 1995. Analysis of a regional model (EURAD) near
744 surface gas concentration predictions using observations from networks. *Meteorol. Atmos.*
745 *Phys.* 57, 173–200.
- 746 Hirst, J.M., 1952. An automatic volumetric spore trap. *Ann. Appl. Biol.* 39, 257–265.
747 doi:10.1111/j.1744-7348.1952.tb00904.x
- 748 Holtzlag, A.A., Nieuwstadt, F.T.M., 1986. Scaling the atmospheric boundary layer. *Bound. Layer*
749 *Meteorol.* 36, 201–209.
- 750 Johansson, L., Epitropou, V., Karatzas, K., Karppinen, A., Wanner, L., Vrochidis, S., Bassoukos,
751 A., Kukkonen, J., Kompatsiaris, I., 2015. Fusion of meteorological and air quality data
752 extracted from the web for personalized environmental information services. *Environ. Model.*
753 *Softw.* 64, 143–155. doi:10.1016/j.envsoft.2014.11.021
- 754 Josse, B., Simon, P., Peuch, V., 2004. Radon global simulations with the multiscale chemistry and
755 transport model MOCAGE. *Tellus B* 56, 339–356.
- 756 Jäger, S., Mandroli, P., Spieksma, F., Emberlin, J., Hjelmroos, M., Rantio-Lehtimäki, A., Al, E.,
757 1995. *News. Aerobiologia (Bologna)*. 11, 69–70.
- 758 Kalyoncu, A., Qoplii, L., Selguk, Z., Emri, A., Kolagan, B., Kocabas, A., 1995. Survey of the
759 allergic status of patients with bronchial asthma in Turkey : a multicenter study. *Allergy* 50,
760 451–456.
- 761 Kouznetsov, R., Sofiev, M., 2012. A methodology for evaluation of vertical dispersion and dry
762 deposition of atmospheric aerosols. *J. Geophys. Res.* 117. doi:doi:10.1029/2011JD016366
- 763 Kukkonen, J., Olsson, T., Schultz, D.M., Baklanov, a., Klein, T., Miranda, a. I., Monteiro, a.,
764 Hirtl, M., Tarvainen, V., Boy, M., Peuch, V.-H., Poupkou, a., Kioutsioukis, I., Finardi, S.,
765 Sofiev, M., Sokhi, R., Lehtinen, K.E.J., Karatzas, K., San José, R., Astitha, M., Kallos, G.,
766 Schaap, M., Reimer, E., Jakobs, H., Eben, K., 2012. A review of operational, regional-scale,
767 chemical weather forecasting models in Europe. *Atmos. Chem. Phys.* 12, 1–87.
768 doi:10.5194/acp-12-1-2012
- 769 Langner, J., Bergström, R., Pleijel, K., 1998. European scale modeling of sulphur, oxidized nitrogen
770 and photochemical oxidants. Model dependent development av evaluation for the 1994
771 growing season. Norkoping.
- 772 Linkosalo, T., Ranta, H., Oksanen, A., Siljamo, P., Luomajoki, A., Kukkonen, J., Sofiev, M., 2010.
773 A double-threshold temperature sum model for predicting the flowering duration and relative
774 intensity of *Betula pendula* and *B. pubescens*. *Agric. For. Meteorol.* 6–11.
775 doi:10.1016/j.agrformet.2010.08.007
- 776 Louis, J.-F., 1979. A parametric model of vertical eddy fluxes in the atmosphere. *Bound. Layer*
777 *Meteorol.* 17, 187–202.
- 778 Loureiro, G., Rabaca, M.A., Blanco, B., Andrade, S., Chieira, C., Pereira, C., 2005. Aeroallergens'

- 779 sensitization in an allergic paediatric population of Cova da Beira, Portugal. *Allergol.*
780 *Immunopathol. (Madr)*. 33, 192–198.
- 781 Mandrioli, P., Comtois, P., V., L. (Eds.), 1998. *Methods in Aerobiology*. Pitagora Editrice,
782 Bologna.
- 783 Marécal, V., Peuch, V.-H., Andersson, C., Andersson, S., Arteta, J., Beekmann, M., Benedictow,
784 A., Bergström, R., Bessagnet, B., Cansado, A., Chéroux, F., Colette, A., Coman, A., Curier,
785 R.L., Denier van der Gon, H. a. C., Drouin, A., Elbern, H., Emili, E., Engelen, R.J., Eskes,
786 H.J., Foret, G., Friese, E., Gauss, M., Giannaros, C., Guth, J., Joly, M., Jaumouillé, E., Josse,
787 B., Kadygrov, N., Kaiser, J.W., Krajsek, K., Kuenen, J., Kumar, U., Liora, N., Lopez, E.,
788 Malherbe, L., Martinez, I., Melas, D., Meleux, F., Menut, L., Moinat, P., Morales, T.,
789 Parmentier, J., Piacentini, A., Plu, M., Poupkou, A., Queguiner, S., Robertson, L., Rouïl, L.,
790 Schaap, M., Segers, A., Sofiev, M., Thomas, M., Timmermans, R., Valdebenito, Á., van
791 Velthoven, P., van Versendaal, R., Vira, J., Ung, A., 2015. A regional air quality forecasting
792 system over Europe: the MACC-II daily ensemble production. *Geosci. Model Dev.* 8, 2777–
793 2813. doi:10.5194/gmd-8-2777-2015
- 794 Martet, M., Peuch, V.-H., Laurent, B., B., M., Bergametti, G., 2009. Evaluation of long-range
795 transport and deposition of desert dust with the CTM Mocage. *Tellus B* 61, 449–463.
- 796 Masson, V., Champelaux, J.-L., Chauvin, F., Meriguet, C., Lacaze, R., 2003. A Global Database of
797 Land Surface Parameters at 1-km Resolution in Meteorological and Climate Models. *J. Clim.*
798 16, 1261–1282.
- 799 Memmesheimer, M., Friese, E., Ebel, A., Jakobs, H.J., Feldmann, H., Kessler, C., Piekorz, G.,
800 2004. Long-term simulations of particulate matter in Europe on different scales using
801 sequential nesting of a regional model. *Int. J. Environ. Pollut.* 22, 108–132.
- 802 Moriondo, M., Orlandini, S. De, P., N., Mandrioli, P., 2001. Effect of agrometeorological
803 parameters on the phenology of pollen emission and production of olive trees (*Olea europea*
804 L.). *Aerobiologia (Bologna)*. 225–232. doi:doi:10.1023/A:1011893411266
- 805 Negrini, A.C., Ariano, R., Delbono, G., Ebbli, A., Quaglia, A., Arobba, D., Allergologia, A., Paolo,
806 O.S., Ligure, P., Sv, I.-P.L., 1992. Incidence of sensitisation to the pollens of Urticaceae (
807 *Parietaria*), Poaceae and Oleaceae (*Olea europaea*) and pollen rain in Liguria (Italy).
808 *Aerobiologia (Bologna)*. 8, 355–358.
- 809 Orlandi, F., Lanari, D., Romano, B., Fornaciari, M., 2006. New model to predict the timing of olive
810 (*Olea europaea*) flowering: a case study in central Italy. *New Zeal. J. Crop Hortic. Sci.* 34, 93–
811 99. doi:10.1080/01140671.2006.9514392
- 812 Orlandi, F., Romano, B., Fornaciari, M., 2005a. Effective pollination period estimation in olive
813 (*Olea europaea* L.): A pollen monitoring application. *Sci. Hortic. (Amsterdam)*. 313–318.
814 doi:doi:10.1016/j.scienta.2005.01.012
- 815 Orlandi, F., Vazquez, L.M., Ruga, L., Bonofiglio, T., Fornaciari, M., Garcia-Mozo, H., Domínguez,
816 E., Romano, B., Galan, C., 2005b. Bioclimatic requirements for olive flowering in two
817 mediterranean regions located at the same latitude (Andalucia, Spain, and Sicily, Italy). *Ann.*
818 *Agric. Environ. Med.* 47–52.
- 819 Oteros, J., Garcia-Mozo, H., Vazquez, L., Mestre, A., Dominguez-Vilches, E., Galan, C., 2013.
820 Modelling olive phenological response to weather and topography. *Agric. Ecosyst. Environ.*
821 179, 62–68.
- 822 Oteros, J., García-Mozo, H., Alcázar, P., Belmonte, J., Bermejo, D., Boi, M., Cariñanos, P., Díaz de

- 823 la Guardia, C., Fernández-González, D., González-Minero, F., Gutiérrez-Bustillo, A.M.,
824 Moreno-Grau, S., Pérez-Badia, R., Rodríguez-Rajo, F.J., Ruíz-Valenzuela, L., Suárez-Pérez,
825 J., Trigo, M.M., Domínguez-Vilches, E., Galán, C., 2015. A new method for determining the
826 sources of airborne particles. *J. Environ. Manage.* 155, 212–218.
- 827 Oteros, J., Orlandi, F., Aguilera, F., Ben, A., Bonofiglio, T., 2014. Better prediction of
828 Mediterranean olive production using pollen-based models. *Agron. Sustain. Dev.* 34, 685–694.
829 doi:10.1007/s13593-013-0198-x
- 830 Oteros, J., Pusch, G., Weichenmeier, I., Heimann, U., Möller, R., Röseler, S., Traidl-Hoffmann, C.,
831 Schmidt-Weber, C., Buters, J.T.M., 2015. Automatic and online pollen monitoring. *Int. Arch.*
832 *Allergy Immunol.* 167, 158–166. doi:10.1159/000436968
- 833 Pereira, C., Valero, A., Loureiro, C., Dávila, I., 2006. IBERIAN STUDY OF AEROALLERGENS
834 SENSITISATION IN ALLERGIC RHINITIS. *Eur. Ann. Allergy Clin. Immunol.* 38, 186–194.
- 835 Petroff, A., Zhang, L., 2010. Development and application of a size-resolved particle dry deposition
836 scheme for application in aerosol transport models. *Geosci. Model Dev.* 3, 753–769. doi:doi:
837 10.5197/gmd-3-753-2010
- 838 Potempski, S., Galmarini, S., 2009. and Physics Est modus in rebus : analytical properties of multi-
839 model ensembles. *Atmos. Chem. Phys.* 9, 9471–9489.
- 840 Prank, M., Chapman, D.S., Bullock, J.M., Belmonte, J., Berger, U., Dahl, A., Jäger, S.,
841 Kovtunen, I., Magyar, D., Niemelä, S., Rantio-Lehtimäki, A., Rodinkova, V., Sauliene, I.,
842 Severova, E., Sikoparija, B., Sofiev, M., 2013. An operational model for forecasting ragweed
843 pollen release and dispersion in Europe. *Agric. For. Meteorol.* 182–183, 43–53.
844 doi:10.1016/j.agrformet.2013.08.003
- 845 Ritenberga, O., Sofiev, M., Kirillova, V., Kalnina, L., Genikhovich, E., 2016. Statistical modelling
846 of non-stationary processes of atmospheric pollution from natural sources : example of birch
847 pollen. *Agric. For. Meteorol.* 226–227, 96–107. doi:10.1016/j.agrformet.2016.05.016
- 848 Ritenberga, O., Sofiev, M., Kirillova, V., Kalnina, L., Genikhovich, E., 2016. Statistical modelling
849 of non-stationary processes of atmospheric pollution from natural sources: Example of birch
850 pollen. *Agric. For. Meteorol.* 226–227. doi:10.1016/j.agrformet.2016.05.016
- 851 Robertson, L., Langner, J., 1999. An Eulerian Limited-Area Atmospheric Transport Model. *J. Appl.*
852 *Meteorol.* 38, 190–210.
- 853 Rojo, J., Orlandi, F., Perez-Badia, R., Aguilera, F., Ben Dhiab, A., Bouziane, H., Diaz de la
854 Guardia, C., Galan, C., Gutierrez-Bustillo, A.M., Moreno-Grau, S., Msallem, M., Trigo, M.M.,
855 Fornaciari, M., 2016. Modeling olive pollen intensity in the Mediterranean region through
856 analysis of emission sources. *Sci. Total Environ.* 551–552, 73–82.
857 doi:10.1016/j.scitotenv.2016.01.193
- 858 Rojo, J., Pérez-Badia, R., 2015. Spatiotemporal analysis of olive flowering using geostatistical
859 techniques. *Sci. Total Environ.* 505, 860–869.
- 860 Sánchez-Mesa, J.A., Serrano, P., Cariñanos, P., Prieto-Baena, J., Moreno, C., Guerra, F., Galan, C.,
861 2005. Pollen allergy in Cordoba city: frequency of sensitization and relation with antihistamine
862 sales. *J. Investig. Allergol. Clin. Immunol.* 15, 50–56.
- 863 Schaap, M., Timmermans, R. M. A., Roemer, M., Boersen, G.A.C., Builtjes, P.J.H., Sauter, F.J.,
864 Velders, G.J.M., Beck, J.P., 2008. The LOTOS-EUROS model: Description, validation and
865 latest developments. *Int. J. Environ. Pollut.* 32, 270–290.

- 866 Scott, B.C., 1979. Parameterization of sulphate removal by precipitation. *J. Appl. Meteorol.* 17,
867 11275–11389.
- 868 Seinfeld, J.H., Pandis, S.N., 1998. *Atmospheric Chemistry and Physics*, 1st ed. Wiley, New York.
- 869 Siljamo, P., Sofiev, M., Ranta, H., Linkosalo, T., Kubin, E., Ahas, R., Genikhovich, E., Jatczak, K.,
870 Jato, V., Nekovar, J., Minin, A., Severova, E., Shalabova, V., 2008. Representativeness of
871 point-wise phenological *Betula* data collected in different parts of Europe. *Glob. Ecol.*
872 *Biogeogr.* 17, 489–502. doi:10.1111/j.1466-8238.2008.00383.x
- 873 Simpson, D., Benedictow, a., Berge, H., Bergström, R., Emberson, L.D., Fagerli, H., Flechard,
874 C.R., Hayman, G.D., Gauss, M., Jonson, J.E., Jenkin, M.E., Nyíri, a., Richter, C., Semeena,
875 V.S., Tsyro, S., Tuovinen, J.-P., Valdebenito, Á., Wind, P., 2012. The EMEP MSC-W
876 chemical transport model – technical description. *Atmos. Chem. Phys.* 12, 7825–7865.
877 doi:10.5194/acp-12-7825-2012
- 878 Simpson, D., Fagerli, H., Jonson, J.E., Tsyro, S., Wind, P., Tuovinen, J.-P., 2003. Transboundary
879 Acidification, Eutrophication and Ground Level Ozone in Europe, Part 1: Unified EMEP
880 Model Description. EMEP Report 1/2003. Oslo.
- 881 Sofiev, M., 2016. On impact of transport conditions on variability of the seasonal pollen index.
882 *Aerobiologia* (Bologna). doi:10.1007/s10453-016-9459-x
- 883 Sofiev, M., 2002. Extended resistance analogy for construction of the vertical diffusion scheme for
884 dispersion models. *J. Geophys. Res.* 107, ACH 10-1–ACH 10-8. doi:10.1029/2001JD001233
- 885 Sofiev, M., Berger, U., Prank, M., Vira, J., Arteta, J., Belmonte, J., Bergmann, K.C., Charoux, F.,
886 Elbern, H., Friese, E., Galan, C., Gehrig, R., Khvorostyanov, D., Kranenburg, R., Kumar, U.,
887 Marecal, V., Meleux, F., Menut, L., Pessi, A.-M., Robertson, L., Rittenberga, O., Rodinkova,
888 V., Saarto, A., Segers, A., Severova, E., Sauliene, I., Siljamo, P., Steensen, B.M., Teinmaa,
889 E., Thibaudon, M., Peuch, V.-H., 2015. MACC regional multi-model ensemble simulations of
890 birch pollen dispersion in Europe. *Atmos. Chem. Phys.* 15, 8115–8130. doi:10.5194/acp-15-
891 8115-2015
- 892 Sofiev, M., Siljamo, P., Ranta, H., Linkosalo, T., Jaeger, S., Rasmussen, A., Rantio-Lehtimäki, A.,
893 Severova, E., Kukkonen, J., 2012. A numerical model of birch pollen emission and dispersion
894 in the atmosphere. Description of the emission module. *Int. J. Biometeorol.* 57, 54–58.
895 doi:10.1007/s00484-012-0532-z
- 896 Sofiev, M., Siljamo, P., Valkama, I., Ilvonen, M., Kukkonen, J., 2006. A dispersion modelling
897 system SILAM and its evaluation against ETEX data. *Atmos. Environ.* 40, 674–685.
898 doi:10.1016/j.atmosenv.2005.09.069
- 899 Sofiev, M., Vira, J., Kouznetsov, R., Prank, M., Soares, J., Genikhovich, E., 2015. Construction of
900 the SILAM Eulerian atmospheric dispersion model based on the advection algorithm of
901 Michael Galperin. *Geosci. Model Dev.* 8. doi:10.5194/gmd-8-3497-2015
- 902 Spano, D., Cesaraccio, C., Duce, P., Snyder, R.L., 1999. Phenological stages of natural species and
903 their use as climate indicators. *Int. J. Biometeorol.* 124–133. doi:doi:10.1007/s004840050095
- 904 Spiekma, F.T., 1990. Pollinosis in Europe: New observations and developments. *Rev. Palaeobot.*
905 *Palynol.* 64, 35–40.
- 906 Udvardy, O., Tedeschini, E., Sofiev, M., Palamarchuk, J., Makra, L., Kajtor-Apatini, D., Magyar,
907 D., 2017. Utazo Allergenek Mediterran eredetu viragpor Magyarorszagon (in Hungarian).
908 *Allergologia* June, 25–27.

- 909 Venkatram, A., 1978. Estimating the convective velocity scale for diffusion applications. *Bound.*
910 *Layer Meteorol.* 15, 447–452.
- 911 Walcek, C.J., Aleksic, N.M., 1998. A simple but accurate mass conservative, peak-preserving,
912 mixing ratio bounded advection algorithm with FORTRAN code. *Atmos. Environ.* 32, 3863–
913 3880. doi:10.1016/S1352-2310(98)00099-5
- 914 Williamson, D.L., Rasch, P., 1989. Two-Dimensional Semi-Lagrangian Transport with Shape-
915 Preserving Interpolation. *Am. Meteorol. Soc.* 117, 102–129.
- 916 Zhang, L., Gong, S., Padro, J., Barrie, L., 2001. A size-segregated particle dry deposition scheme
917 for an atmospheric aerosol module. *Atmos. Environ.* 35, 549–560.
- 918
- 919